On the Microstructure-dependency of Mechanical Properties and Failure of Low-Pressure Cold-Sprayed Tungsten Carbide-Nickel Metal Matrix Composite Coatings

Guriqbal Munday, James Hogan, André McDonald*

Department of Mechanical Engineering,
University of Alberta,
10-230 Donadeo Innovation Center for Engineering,
9211-116 Street NW, Edmonton, Alberta, T6G 1H9, Canada

**Corresponding Author - Phone: 1-780-492-2675*
E-mail: andre.mcdonald@ualberta.ca

ABSTRACT

This study improves upon understanding of the effects of reinforcing particle content and microstructure on the mechanical properties and failure of low-pressure cold spray fabricated tungsten carbide-nickel (WC-Ni) metal matrix composite (MMC) coatings. Image analyses were performed on scanning electron microscope (SEM) micrographs of the coatings to characterize the microstructure and measure the total interfacial area between the reinforcing WC particles and the Ni metal matrix, the mean free path between the particles, the average particle size, and the porosity of the coating. Uni-axial quasi-static tensile testing was conducted on the as-sprayed coatings. The tensile stresses that were measured were coupled with the evolving strains that were calculated by using the digital image correlation (DIC) technique. The results showed that mechanical properties, namely tensile strength and Young's modulus, of the composite coatings increased with increasing WC content in the coatings. The increases were due to the refined microstructural features that occurred with the decrease in the porosity of the coating that was caused by significant consolidation of the Ni metal matrix. Furthermore, this increase in strength and Young's modulus was also related to the increase in the interfacial area between the reinforcing carbide particles and the metal matrix that was caused by the increase in carbide content in the coating, a decrease in the average size of the carbides in the coating, and a reduction of the mean free path between the carbide particles. A framework was presented to elicit the micro-macro relationships between the microstructure and the tensile strength of the cold-sprayed composite coatings. Based on the developed framework, two distinct coating mechanical strength regimes were observed, indicating a significant increase in the tensile strength of the coatings that were comprised of more than 30 wt.% WC due to the refined microstructure of the coatings. The higher value tensile strength regime was also confirmed by the larger average mechanical energy absorbed to failure under tensile loading and lower damage accumulation. This collection of data of mechanical properties and the microstructures presented in this study are important to validate numerical-based failure models for cold-sprayed composite coatings. Altogether, the results of this study will enhance understanding of the sensitivity of mechanical response of a composite coating to microstructural changes.

KEYWORDS Cold spray; Metal matrix composite; Microstructure; Tensile testing; Young's modulus

INTRODUCTION

Protection of mechanical equipment against surface degradation processes such as wear, erosion, and corrosion is a challenging task in Oil & Gas, Aerospace, Defense, Mining, and many other industries [1, 2]. Wear of the equipment causes premature failure, resulting in loss of both capital and operation time. Notably, in the Oil & Gas industry, a significant portion of the operating costs are directed to mitigate wear loss due to aggressive wear environments that include hard-faced erodent particles that are present in oil sand slurries [1]. Therefore, to avoid wear and other related detrimental phenomena in harsh environments, equipment surface protection is desired [1, 2].

Surface modification of equipment to withstand the detrimental effects of exposure to wear-dominated environments by employing sacrificial coatings is pervasive in practice [2 – 5].

Generally, these coatings need to have higher hardness, strength, and toughness to survive the highly erosive or abrasive environments to which they will be exposed [1 – 6]. Therefore, in contrast to single phase materials, multi-phase composites or metal matrix composite coatings may have tailored mechanical properties that are better suited for these particularly aggressive environments. MMCs comprise of at least two constituent phases, where one of those phases is metallic or metal alloy, and the other reinforcing phases may be different metals or other materials such as a ceramic, inorganic material, or organic material. Particulate-reinforced MMCs are those in which hard particles are distributed through a typically softer matrix. This combination provides for an expanded field of application over their constituent material components, where the reinforced hard particles typically provide the required stiffness, while the metal binder increases the toughness [5 – 12].

There have been numerous studies on fabricating WC-based MMC coatings to mitigate wear [13 – 16]. These wear-resistant coatings may be applied to the surface being protected using laser cladding, thermal spray, vapor deposition, and electroplating, among many others [2, 3, 9]. However, higher deposition temperature and other related issues such as oxidation, tensile thermal stresses, decarburization, and metallurgical phase transformations limit their use [9, 10, 12, 17]. A relatively new deposition method, cold gas dynamic spraying (or simply, cold spraying) provides a promising alternative to fabricate MMC coatings. In particular, Melendez, *et al.* [13] and Lee, *et al.* [14] have already successfully deposited WC-based wear resistant MMC coatings using a low-pressure cold spraying equipment. Cold spraying is a coating deposition method in which powder particles are accelerated through a de Laval nozzle to between 300 m/s and 1200 m/s. The powder particles deform plastically upon impact, adhere to the substrate, accumulate, and produce a coating on the surface [9, 10, 12]. Thus, with deposition temperatures lower than the melting point of the feedstock powder, the cold spray process provides an alternative method to fabricate coatings that are devoid of defects that are ordinarily present in coatings that are fabricated by other spray processes (e.g., plasma spraying, wire arc spraying, and flame spraying [10]).

Parallel to developing novel coating fabrication methods, many researchers have also focused on refining the microstructure of MMCs in order to design MMC coatings with improved wear and mechanical property performance. Notably, Chawla, *et al.* [6] have showed that microstructural features such as shape, size, and mean free path between the reinforcing particles in a MMC coating significantly affect the macro-mechanical response of those coatings. Similarly, Gustafson, *et al.* [18] and Lee, *et al.* [19] noted that yield strength is a function of mean free path between the particles. Also, Kouzeli, *et al.* [20] reported a significant improvement in the hardness of MMC coatings that had particle mean free paths less than 10 μm. This was also confirmed by Hodder, *et al.* [23] who showed that for Al_2O_3 reinforced MMC coatings, a decrease in mean free path, ameliorated with dislocations, results in higher hardness values of low-pressure cold spray fabricated coatings. Similar observations were also made by Melendez, *et al.* [13] when conducting ASTM Standard G65 dry abrasion wear testing on cold-sprayed tungsten carbide (WC) reinforced nickel (Ni) coatings. They argued that a decrease in mean free path is likely to reduce the probability of interaction between the metal matrix and the hard-abrasive particles. Further, the effect of grain size on the strengthening of metals and failure of brittle materials have been studied broadly, and relationships such as the Hall-Petch and Griffith criteria have shown that, in general, the strength of a metal increases with a decrease in the grain size of the metal [24, 25, 26]. Luo, *et al.* [26] noted that that the strengthening of the high-pressure cold spray fabricated nanocomposites was dependent on the matrix grain size and dislocation density of the matrix. They also showed that for high-pressure cold spray fabricated nanocomposites, the abrasive wear resistance and hardness were dependent on the reinforcing particle size [27]. Similarly, Holmberg, *et al.* [29, 30] have noted the importance of tailoring the microstructure in predicting the wear performance of MMC coatings using numerical simulations. Thus, the influence of microstructure on material and mechanical properties of multiphase materials is widely acknowledged and is one of the critical aspects in the design of MMCs [6, 9, 14 – 30].

Extracting a comprehensive set of mechanical properties data of MMC coatings has always been a challenge due to the anisotropy of the coatings and their attachment to the substrate [31, 32]. Therefore, localized experiments such as micro and nano indentation have been utilized in order to characterize the material properties and performance of the coatings [26, 31]. Thus, based on reported experimental work on MMC coatings, it may be assumed that the hardness of the coating is the sole determinative factor of the wear performance of the coatings [13 – 15, 29, 30]. However, the results obtained by Holmberg, *et al.* [30] from a wear test found weak correlation between the wear rate and the hardness of the particle as well as with that of the matrix. Thus, the characterization of performance based on localized mechanical properties such as hardness could be misleading or overstated. Nonetheless, researchers have begun to understand that in order to comprehend the mechanical response of coatings better, a broader testing protocol of the coatings is of paramount importance [3]. Thus, Vackel, *et al.* [2] conducted tensile tests on thermal-sprayed coatings; however, most of their research was focused on investigating the load sharing between the coating and the substrate and not on analyzing the mechanical properties of the coating material. Other properties such as toughness or the mechanical energy absorbed by the MMC coating material up to the point of failure under loading have been discussed qualitatively by other investigators [13] but have not be quantified widely in previous studies on MMCs.

A complete and foundational understanding of the mechanical response of cold-sprayed coatings under loading and the interaction between the microstructure of the coating and the mechanical response is still lacking. Therefore, the objectives of this study were to: (1) develop a high-strength cold-sprayed metal matrix composite coating by tailoring the carbide content, (2) determine the mechanical properties of the composite by conducting uniaxial tensile tests, and (3) correlate the observed mechanical properties and failure with the microstructure of the coatings. The quantification and assessment of the mechanical properties of cold-sprayed particulate-reinforced MMC coatings will serve to inform their impact on the performance of the coating material to guide the development of next-generation coatings with tailored microstructure.

EXPERIMENTAL PROCEDURE

A mechanically blended powder was used as the feedstock for the metal matrix composite coatings. The powders were prepared based on the weight percentages of tungsten carbide (WC-8245, Pacific Particulate Materials Ltd., Port Moody, BC, Canada) and a commercially pure Ni powder (SST-N5001, CenterLine Ltd., Windsor, ON, Canada), which was particularly designed for cold spraying and was selected as the powder feedstock material for the metal matrix. The size distribution of the as-received WC was -270 mesh (-53 μm), and that of the Ni powder was -45+5 μm (5 to 45 μm). Three different feedstock powder blends were prepared based on 50, 71, and 92 weight percentages of WC in the blend. ~~**The powder feed rate was approximately 10 g/min.**~~ Images of the morphology of the powders have been presented by Lee, *et al*. [14]. The Ni powder was dendritic in structure and the WC particles had angular shapes with sharp edges [14]. Low carbon steel was used as the substrates on which the powder blends were deposited. Prior to deposition of the powder blends, the substrates were roughened by using #24 alumina grit (Manus Abrasive Systems Inc., Edmonton, AB, Canada).

The composite coatings were fabricated by using a portable low-pressure cold spray unit (SST series P, CenterLine, Ltd., Windsor, ON, Canada). The process parameters are summarized in Table 1. The rastering of the spray nozzle was achieved by installing it on an automatic robot (HP-20, Motoman, Yaskawa Electric Corp., Waukegan, IL, USA). This ensured a constant distance between the substrate and the nozzle (the stand-off distance) (see Table 1). **The powder feed rate was approximately 10 g/min.** In all cases, at least four coating samples from each feedstock powder blend were fabricated to confirm repeatability of the deposition process and the resulting coatings.

Uniaxial tests were conducted at room temperature on a material testing system (MTS 810, MTS Systems Corporation, Minneapolis, MN, USA) in order to evaluate the mechanical properties of the fabricated coatings. Tensile test coupons of the coating samples were prepared according to ASTM Standard E8/E8M-13a [35] by using a wire-based electrical discharge machine (Agie Progress V4, Agie, 1242 Satigny, Switzerland) to cut the coatings from the substrate. The samples were machined to sub-sized dog-bone shapes with gauge dimensions of 25 mm × 6 mm. The thickness of the coating samples was 1.2 mm. The selected dimensions of the dog-bone samples were the minimum dimensions that were specified in the Standard and allowed the samples to develop uni-axial strain during external tensile loading on the coatings. The dog-bone samples were loaded at a loading rate of 0.001 mm/s, which placed the test condition in the quasi-static loading regime. Also, the loading direction was parallel to the powder deposition direction.

Advanced imaging techniques were used to measure the deformation of the tested dogbone samples, in lieu of traditional extensometers. This included capturing *in-situ* the deformation using a Promon U750 High Speed Camera (AOS Technologies AG, Taefernstrasse 20 CH-5405 Baden-Daettwil, Switzerland) at 100 frames/s and full resolution of 1280 × 1024 pixels. A video of the deformation event was used to create time-stamped images of the recorded experiment. These images were utilized to compute the longitudinal strains using the digital image correlation (DIC) technique (Vic-2D v6 software, Correlated Solutions, Inc., Irmo, South Carolina, USA). Through this technique, an area of interest as large as the gauge area of the specimen was selected on a reference image, which was generally an image of the unloaded specimen. A rectangular grid was drawn with the Vic-2D software suggested subset size varying between 15 × 15 and 25 × 25 pixels. This grid was digitally tracked in the subsequent time-stamped images, and the software provided the strain as a function of the elapsed time in the tensile tests. In order to reconcile the stress data with the DIC strain data, the failure stress in the dogbone was aligned with the corresponding strain to failure, and afterwards all of the stresses and corresponding strains were aligned to produce stress-strain curves. The Young's moduli of the coatings were determined by calculating the slope of the stress-strain curves that were obtained from the tensile tests.

A scanning electron microscope (EVO 10, Zeiss, Cambridge, UK) was used to capture magnified images of the fabricated coating samples. Image analysis (ImagePro, Media Cybernetics, Bethesda, MD, USA) on the captured micrographs facilitated the characterization of the microstructure of the coating. At least five images were taken of each sample (n = 5). At least five random areas of interest of each image were analyzed to determine the effect of microstructural features of the coating on its properties. The average volume percent (vol.%) of WC in the coatings was determined, which was then converted to weight percent (wt.%) based on the density of WC and Ni, where were 15,800 kg/m^3 and 8,900 kg/m^3, respectively [13]. The procedure to convert vol.% to wt.% is already described in detail by Melendez, *et al.* [13]. The micrographs were used to calculate the mean free path between the reinforcing particles, which is representative of the spacing between the adjacent WC particles. The mean free path was calculated by using [20]

$$\lambda = \frac{1 - v_{\mathrm{r}}}{N_{\mathrm{L}}}, \qquad (1)$$

where v_{r} is the volume fraction of the WC particles and N_{L} is the number of WC particle intercepts per unit length. The N_{L} was calculated by drawing five random lines on the SEM images and the number of particle intercepts with the lines was manually determined. Further, an in-built function in ImagePro software (Area (polygon)) was used to estimate the average WC particle size in the as-sprayed coatings. At least fifty particles were measured per area of interest. Therefore, the standard deviation in the data represents the standard deviation of the average of particle size instead of particle size. Similarly, the total interfacial area per unit thickness between the deposited WC particles and the Ni metal matrix was also estimated using an in-built function in the ImagePro software (Perimeter). Similar to particle size calculations, this was also calculated based on five different areas of interest, selected on five different micrographs per sample (n = 25). The error calculations presented in this study show the standard error of the mean, wherein the standard deviation was divided by the square root of the number of measurements, n.

RESULTS

The present study has focused on the fabrication of an MMC coating using a low-pressure cold spray unit. This was followed by quantification of the mechanical properties of the coating with consideration of possible microstructural effects on the mechanical properties of the fabricated WC-Ni MMC coatings. Figure 1 shows the magnified SEM images of the cross-section of coatings deposited using feedstock powder containing 50 wt.% WC + 50 wt.% Ni, 71 wt.% WC + 29 wt.% Ni, and 92 wt.% WC + 8 wt.% Ni powder blends. Figure 1(a) indicates that the distribution of the WC particles in the matrix was heterogeneous as they were non-uniformly distributed in the metal matrix. However, the distribution of WC in the matrix is such that it is more homogeneous with an increase in content of WC in the coating (see Fig. 1c). Previous studies by Melendez, *et al.* [13] and Lee, *et al.* [14] have already confirmed that the brighter phase in identical micrographs corresponds to the WC particles and the darker phase to the Ni matrix material. Melendez, *et al.* [16] have also used X-ray diffraction analysis to show that by using cold spray deposition parameters that are similar to those used in this present study, decarburization and other thermally-induced phase changes in the WC particles did not occur when the WC powder particles were deposited into the coating.

Figure 2 presents a plot of the weight fraction of WC reinforcing particles in the MMC coatings as a function of weight fraction of WC particles in the feedstock powder. The results suggest that the weight percent of WC increases in the coating with an increase in the wt.% of WC in the feedstock powder. For example, approximately 13 wt.% of WC was deposited when 71 wt.% of WC was in the powder blend (see Fig. 2). These results also show that less WC was deposited in the coating than that which was in the WC in the initial powder blend. This was explained by Irissou, *et al.* [12] and attributed to the fact that the incorporated hard particles do not deform plastically upon impact and, hence, possess an inability to adhere to the surface of the substrate. Similar results for cold spray WC-Ni MMC coatings were obtained by Lee, *et al.* [14].

Figure 3 shows the tensile stress-strain curves that were obtained from the coatings that were fabricated from the three feedstock powder blends. Tensile strength measurements were conducted on the as-sprayed coatings with WC weight fractions varying from approximately 6 wt.% to 40 wt.% (see Fig. 3). The final wt.% of WC in the coating is marked on the plots. Samples without WC particles were not tested in this study because those coatings were highly porous, friable, and difficult to machine into dog-bone shapes. Figure 3 shows that the tensile strength of the MMC coating increases with an increase in WC wt.% in the coating. For comparison, the tensile strength of the MMC coating with 6.35 ± 0.06 wt.% WC was found to be approximately 38 MPa (see Fig. 3a and Table 2); however, when the as-sprayed coating contained approximately 13.69 ± 0.03 wt.% WC, the tensile strength increased to approximately 128 MPa (see Fig. 3b and Table 2), which represented a 236% increase in the tensile strength of the coating. The most significant change in the strengthening effect of the hard-reinforcing particles was observed in the coatings that contained more than 30 wt.% WC. When approximately 34.92 ± 0.03 wt.% WC was present in the MMC coating, the tensile strength was 276 MPa (see Fig. 3c and Table 2).

The slope of the tensile stress-strain curves measured at approximately 0.016% strain was used to compute the Young’s modulus of the coatings. From analysis of the curves shown in Fig. 3 and Young’s modulus data presented in Table 2, the Young’s modulus increased steadily with an increase in WC content in the coatings. As shown in Table 2, the Young’s modulus of the coating with 6.35 ± 0.06 wt.% WC was approximately 121 GPa and increased to 233 GPa for coatings with WC content above 30 wt.% at 34.92 ± 0.03 wt.% WC.

The tensile failure strains that were measured also changed as a function of WC content in the coatings. Figure 3 shows that the tensile failure strains increased with an increase in the WC content in the coatings. For comparison, the tensile failure strain of the coating with 7.69 ± 0.07 wt.% WC was found to be approximately 0.08% (see Fig. 3a and Table 2), while for the coating with approximately 11.47 ± 0.04 wt.% WC, the failure strains increased to 0.11% (see Fig. 3b and Table 2). As the content of WC in the coating increased beyond 30 wt.% to 34.92 ± 0.03 wt.%, the failure strain increased to 0.14% (see Fig. 3c and Table 2).

The mechanical energy absorbed to failure by the coatings, which is equivalent to toughness, was determined by calculating the area under the tensile stress-strain curves. The values obtained from the measurements represent the energy absorbed to failure of lamellar coating material systems that have reinforcing particles and pores distributed through them. From analysis of the curves shown in Fig. 3 and data presented in Table 2, the toughness of the coatings increased with an increase in WC content in the coatings. For comparison, the toughness of the coating with 7.69 ± 0.07 wt.% WC was found to be approximately 0.03 N/mm^2, while for the coating with approximately 11.47 ± 0.04 wt.% WC, the toughness increased to 0.07 N/mm^2. As the content of WC in the coating increased beyond 30 wt.% to 34.92 ± 0.03 wt.%, the toughness increased to 0.2 N/mm^2.

DISCUSSION

Effect of carbide content on mechanical properties

The observed changes in the mechanical and material properties of the cold-sprayed MMC coatings was likely influenced by the coating microstructure that was developed during deposition of the powder blends to fabricate the coatings. The observed increase in the tensile strength and other mechanical properties of the composite coatings were primarily a result of an increase in the content of WC particles in the coating among other contributing microstructural effects. In multi-phase particulate-reinforced composite materials, the strength of the material has been shown generally to increase as a result of load sharing among the particulate inclusions in the matrix [6, 11]. In this study, the effect of an increase in the content of WC in the coating on changes in the mechanical properties has been characterized by calculating the total interfacial area (Ψ) between the WC reinforcing particles and the metal matrix. Primarily, Ψ was the area available to transfer and share load from the matrix to the stiffer carbide during application of external loading. Figure 4 shows the plot of tensile strength as the function of Ψ. In particular, a coating containing 7.69 wt. ± 0.07 % WC had a total interfacial area per unit thickness of approximately 7,018 ± 214 μm, while a coating containing 40.47 ± 0.03 wt.% WC had a total interfacial area per unit thickness of approximately 35,524 ± 3960 μm (see Table 3) . As shown in Fig. 4, as the interfacial area increased, the overall tensile strength of the coating material increased, such that there was an approximate direct relationship between the tensile strength and Ψ, which may be represented as,

$$\sigma \propto \psi \,, \tag{2}$$

where σ is the tensile strength and Ψ is the total interfacial area per unit thickness between the WC reinforcing particles and the metal matrix of the coating. This phenomenon of increase in the values of the mechanical properties of the cold-sprayed WC-Ni MMC coatings with an increase in WC content in the coatings was recognized as direct strengthening of the MMC coating [11, 26, 36]. Under tensile loading, with an increase in the WC in the fabricated MMC coatings, a larger external load was transferred from the matrix to the stiffer WC particle reinforcements, producing an overall composite medium coating that possessed improved tensile strength.

Effect of mean free path on mechanical properties

The improvement in the mechanical properties of the cold spray fabricated MMC coatings that had higher WC content in the coatings is also dependent on the mean free path (λ) between the reinforcing particles in the matrix, which is the spacing between particles. Table 3 shows the calculated values of λ. It was observed that with an increase in the content of WC in the coatings, there was a decrease in the mean free path (see Table 3). For example, for a coating containing 6.35 ± 0.06 wt.% WC, the mean free path is 83 ± 10 μm, compared to the mean free path of 12 ± 0.4 μm at 37.78 ± 0.04 wt.% WC in the coating. The effect of λ on the strength of the composites was also studied by Gustafson, *et al.* [18] and Lee, *et al.* [19]. They described a functional relationship between the strength and λ and reported a linear increase in strength as a function of $\frac{1}{\sqrt{\lambda}}$. For the composites that were tested in this study, the curve of this relationship was plotted in Fig. 5 and it shows that with a decrease in the mean free path, there was an increase in the tensile strength of the composite. Figure 5 shows good agreement with the proposed framework as it shows a nearly linear relationship between the tensile strength of the as-sprayed MMC coating and $\frac{1}{\sqrt{\lambda}}$. This relationship is represented as,

$$\sigma \propto \frac{1}{\sqrt{\lambda}}. \tag{3}$$

The coatings with lower λ and which contained more homogeneously distributed particles due to the higher particle content possessed higher tensile strength. The reduction in the mean free path between the particles may have imposed greater constraints on plastic deformation of the metal matrix of the coating under loading and hence limited the coalescence of any nucleated voids that would develop under external loading [6, 36]. The nucleated voids that did not coalesce were likely able to inhibit the propagation of cracks through the MMC coating, resulting in increase of the strain to failure and ultimately the tensile strength of the coating.

Effect of WC particle size on mechanical properties

Changes in the mechanical properties of the cold-sprayed MMC coatings may also be attributed to changes in the equivalent particle diameters of the WC in the coatings [26]. Given the irregular morphology of the WC particles (see Fig. 6), the average area of the particles in the coating was selected to study the effect of particle size [37]. During the cold spray process, powder particles undergo fracture upon impact on the substrate and previously deposited layers, resulting in size reduction of the particles [12 – 14]. Table 3 shows the average reinforcing particle size (ϕ) in the fabricated coatings. There was a decrease in the average reinforcing particle size from approximately 19.37 ± 0.44 μm^2 at 6.35 ± 0.06 wt.% WC in the coating to approximately 8.64 ± 0.29 μm^2 at 37.78 ± 0.04 wt.% WC in the coating (see Table 3). Empirical relationships for metals based on the Griffith criteria for fracture [24] and Hall-Petch relationship [25] have shown that the strength of metals varies as the inverse of the square root of the crack size and the metal grain size, respectively. Also, for MMCs, Nan, *et al.* [28] reported that the strength varies as the inverse of the square root of the size of the reinforcing particle. This motivated speculation in this study toward a similar relationship between the tensile strength and the particle size of the cold-sprayed WC-Ni MMC coatings, which is given as

$$\sigma \propto \frac{1}{\sqrt{\phi}}, \tag{4}$$

where σ is the tensile strength and ϕ is the average particle size in the coating. The curve of this relationship is plotted in Fig. 7 and it shows that with a decrease in the average particle size, there is an increase in the tensile strength of the composite.

Smaller average WC particle sizes allow for lower particle mean free path and increased strengthening of the MMC coating. Besides, during the cold-spray of carbide particles, strengthening may be attributed to dislocation pile-up in both the metal matrix and the reinforcing particles [26]. The metallic matrix experiences intense plastic deformation during cold spray deposition of carbide particles, which results in work-hardening and grain refinement of the matrix [26]. Investigators such as Luo, *et al.* [26] and Dewar, *et al*. [39] have shown that for low-pressure cold-spray deposition of metals, localized grain refinement close to the point of impact of the particles occurs.

Similarly, dislocations are generated in the WC particles due to high strain rate impact of WC particles during deposition and lead to further strengthening of the composite [20, 23, 26, 36, 38]. In addition, smaller WC particle sizes may also augment the strengthening due to the increase in the number of dislocations in the fabricated coatings [20, 21, 26]. Kouzeli, *et al.* [20] differentiated the dislocations as geometrically necessary dislocations (GNDs) and statistically stored dislocations (SSDs). GNDs are formed during external loading of an MMC [20]. They are stored in the MMC due to its non-uniform deformation and are generally necessary for compatible deformation of the MMC [20]. Conversely, SSDs are formed due to the characteristics of the manufacturing process [20]. An increase in the content of WC in the cold spray feedstock powder, increases the probability of SSDs, as a higher number of WC particles impact on the previously deposited powder layers. Therefore, a decrease in average particle sizes would result in an increase in the number of dislocations because smaller particle sizes may potentially increase the number of locations available for the generation of dislocations. Though difficult to quantify in the present experiments, dislocations likely play a significant role in the indirect strengthening of the metal matrix [9, 23].

Effect of porosity on mechanical properties

The SEM micrographs that were taken of the coating cross sections were also used to evaluate the porosity (θ) of the coatings (see Fig. 1). Table 3 shows the calculated values of the porosity of the fabricated WC-Ni MMC coating. The data indicates that there was a decrease in porosity of the coating with an increase in the content of WC in the feedstock powder and subsequent increase in the fabricated WC-Ni MMC coating. For example, the porosity of the coating with approximately 6.35 ± 0.06 wt.% WC was approximately 0.48 ± 0.03 vol.% and decreased to 0.037 ± 0.004 vol.% porosity when the WC content in the coating was increased to 34.92 ± 0.03 wt.% (see Table 3). Figure 8 shows the curve of tensile strength as a function of porosity of the coating. The trend in the figure suggests that there is an inverse relationship between the tensile strength and the porosity of the coating. This may also be represented in equation form as,

$$\sigma \propto \frac{1}{\theta}, \tag{5}$$

where σ is the tensile strength and θ is the porosity in the coating. This reduction in the porosity may have resulted from the effect of in-situ peening of the coating during repeated impact of carbide particles on the substrate and previously deposited metal matrix composite layer, producing a highly dense metal matrix with reduced three dimensional defects such as pores [13, 14]. This increased consolidation of the metal matrix may have resulted in better load transfer from the matrix to the stiffer carbide [26]. Unlike the data shown in Figs. 5 and 7, the data shown in Fig. 8 is not amenable to curve fitting due to the singular change in tensile strength as the porosity decreases.

The effect of microstructural features on the mechanical and materials properties of MMC coatings is rarely independent, and each one may act in concert with the others. In this study, the total interfacial area between the WC reinforcing particles and the metal matrix, the mean free path between the reinforcing particles, the average particle size, and the coating porosity are inter-dependent in terms of their effect on the mechanical and materials properties of MMC coating. Given the functional relationships that were presented in Eqs. (2) to (5), a functional relation among the dependent variable tensile stress and the independent variable of interfacial area, mean free path, average particle size, and coating porosity may be shown. Thus, Eq. 6 provides that

$$\sigma \propto \frac{\psi}{\sqrt{\phi} \times \sqrt{\lambda} \times \theta}. \tag{6}$$

This functional relationship, as shown in Fig. 9, suggests that there were two different regimes, which were distinguished when the content of WC in the coating was less than approximately 15 wt.% (left curve) and when the content was more than 30 wt.% (right curve). For the regime that is governed by coating WC content less than 15 wt.%, there is an approximately linear relationship between the tensile strength and the independent variables, with an *R*-squared value of 0.94 (see Fig. 9). A similar investigation at higher WC content (see Fig. 9) also suggests an approximately linear relation between tensile strength and the independent variables, with an *R*-squared value of 0.94. The trends that are observed in both the curves of Fig. 9 suggest that the increase in the tensile strength may be partly due to the decrease of pores in the as-sprayed cold-sprayed coatings. It is likely that at lower WC content in the coatings, porosity plays a substantive role in the failure of the matrix. At higher porosity, due to external loading, there is a high volume of collapsing of pores due to lateral compression which results in higher initial damage accumulation and hence lower strength. This lower strength at higher porosity is also evident from the mechanical energy absorbed to failure by the samples during external loading. For the coatings with higher porosity and WC content less than 15 wt.%, the average energy absorbed is approximately 0.04 ± 0.02 N/mm^2 (n = 8). In contrast, cold-sprayed coatings with lower porosity and with WC content greater than 30 wt.% may behave like solid material and may have less damage accumulation, explaining their higher strength. This higher strength is also manifested in the larger average mechanical energy absorbed to failure, which is approximately 0.13 ± 0.06 N/mm^2 (n = 4).

The effect of porosity on the damage and failure of the coatings was explored by analyzing the lateral strains as a function of the axial strains of the coatings (see Fig. 10). The calculation of lateral strains was made feasible by utilizing the DIC technique, which was otherwise difficult to calculate by using traditional extensometers. The plot in Fig. 10a demonstrates that there was specimen to specimen variation in the lateral strains for the tested composite coatings. Singh, *et al.* [40] studied lateral strains for silicon carbide-reinforced aluminum MMC and attributed this variation to the varied content of reinforcement content, particle shape, size, and their agglomeration or clustering in the MMC. Thus, evolution of the lateral strains is dependent on the microstructure of the MMC and as observed in Fig. 10a, as the axial strain increases, the shape of the curves becomes irregular. This indicates that damage in the coatings has occurred. Also, as the axial strain approaches the failure strain, there was a dramatic change in the slope of the curves. To analyze the failure in the MMC further, Singh, *et al.* [40] studied the Poisson's ratio and noted that it might be utilized as an indicator to study damage in the composites.

Poisson' ratio is a fundamental mechanical property that is used to study the convoluting behavior of the microstructure of a material and its influence on the macro-mechanical response of a material [41]; however, minimal studies have reported the Poisson's ratio for cold-sprayed MMC coatings. Poisson's ratio is defined as the absolute ratio of the lateral strain to the axial strain in the elastic loading regime [40–42]. The evolution of lateral strains as a function of axial strains, or the Poisson's ratio, promotes an understanding of the dimensional changes of materials under external loading [40–42]. In this study, the absolute value of the slope of the curves shown in Fig. 10, which is equivalent to Poisson's ratio, was investigated at approximately 0.006% axial strain. For the coatings with WC particle content less than 15 wt.% (see Fig. 10, solid curves), the calculated average of the Poisson's ratio was 0.41 ± 0.24 (n = 8). In contrast, for coatings with WC particle content more than 30 wt.% (see Fig. 10, dashed curves), the average of the Poisson's ratio was 0.23 ± 0.06 (n = 4). The sources of this difference in Poisson's ratio with a change in WC content in the coating are explained as follows.

The Poisson's ratio of bulk, pure Ni is 0.31 [42, 43] and that of WC is 0.22 [42]. Since WC has lower Poisson's ratio, it follows from the definition of Poisson's ratio that under external loading, the WC particles would undergo smaller dimensional changes than the Ni [40]. Similarly, for a composite fabricated using WC particles and Ni metal matrix, under tensile loading, the dimensional changes will be more for Ni metal matrix, than for the WC particles. In other words, the Ni metal matrix will have greater tendency to deform laterally than the WC particles. For a given axial strain, this inward lateral displacement of the Ni metal matrix in the WC-Ni MMC coatings may be due to the porosity in the coating, which is also a function of the WC content in the cold-sprayed MMC coatings. In a coating with higher initial porosity and lower WC content, the lateral displacement of material under loading would fill the pores and hence, enable deformation of the Ni metal matrix. Due to this higher lateral displacement in a coating with higher porosity and lower WC content, damage in the composite would increase, and damage accumulation would be imminent [40]. This suggests that coatings with higher Poisson's ratio would indicate greater damage during loading [40].

Since the WC content and porosity in the coating directly affects the tensile strength of the cold-sprayed WC-Ni MMC coating, it is plausible that changes in the Poisson's ratio due to variations in the WC content and porosity in the coating may provide another parameter to explain the observed variations in the tensile strength of the cold-sprayed MMC coatings. Based on the previous explanation of damage, it may be inferred that a coating with higher Poisson's ratio, which is indicative of higher damage accumulation, should fail at a lower tensile stress compared to a coating with lower Poisson's ratio. It was observed in this study that for a coating with 11.47 ± 0.04 wt.% WC and 0.42 ± 0.06 vol.% porosity, the Poisson's ratio was approximately 0.38 and the calculated tensile strength was 110 MPa. In comparison, for a coating with a higher WC content of 37.78 ± 0.04 wt.% and 0.042 ± 0.005 vol.% porosity, the Poisson's ratio decreased to 0.15 and had a higher tensile strength of 257 MPa. Thus, it was observed that for a high value of Poisson's ratio of the cold-sprayed WC-Ni MMC coating, the tensile strength was lower.

The comparison of the average Poisson's ratio for the two different WC contents in the coating suggests that porosity may influence the damage and failure of the tested coatings. However, Fig. 10b appears to suggest that damage and failure of the coatings may not be exclusively dependent on the porosity of the coatings. For example, for a coating with 6.45 ± 0.11 wt.% WC and 0.35 ± 0.03 vol.% porosity, the Poisson's ratio was 0.18, compared to the higher Poisson's ratio of 0.33 at 40.47 ± 0.03 wt.% WC and 0.049 ± 0.006 vol.% porosity (see Fig. 10b). Hence, as indicated in Fig. 10b, there was higher damage accumulation in the coating with higher WC content and lower porosity, which should be followed by lower tensile strength. However, the tensile strength of the coating with 40.47 ± 0.03 wt.% WC was 220 MPa, compared to 72 MPa at 6.45 ± 0.11 wt.% WC in the coating (see Table 2). Therefore, the explanation of the damage and failure of the cold-sprayed WC-Ni coatings as dependent solely on the porosity would be inappropriate. Holmberg, *et al.* [28], also reported that, in addition to the porosity, the localized influence of other microstructural features such as the particle-particle mean free path, the reinforcing particle size, and defects also affect the mechanical properties of the coatings. In addition, they noted that defects were a critical feature that affected the wear and mechanical properties of the thermally sprayed coatings. Similarly, Fig. 10 suggests that damage and failure of the cold-sprayed WC-Ni coatings may be influenced by a combination of microstructural features [29, 33, 34]. This reinforces the significance of examining the combined effect of microstructure, as highlighted by the results of Eq. 6. Further analysis is needed; however, Eq. 6 may provide preliminary indications of the interaction between microstructure and tensile strength of cold-sprayed WC-Ni MMC coatings.

The data collected in this study on the mechanical properties (e.g., Young's modulus, tensile strength, toughness, and Poisson's ratio) and the microstructural features (e.g., porosity, particle-particle mean free path, and average particle size) may be used to advance understanding and aid other investigators to establish and validate mechanism-based numerical models. There are studies that focused on modelling the mechanical response of thermal-sprayed coatings [29], laser-cladded coatings [29], and ceramic-metal materials [50]; however, no explicit numerical model is available for the coatings fabricated using the cold spraying process. In general, as noted by Holmberg, *et al.* [29, 30], a modelled solution may provide insight into the dominating features that impact the mechanical properties and performance of the coatings. The constitutive equations based on the asymptotic homogenization and mean field approach may be used to solve the discretized microstructure [46]. Since these homogenization techniques do not include the effect of porosity, size, shape, and orientation of the particle phase in the composite, their use is limited to modelling only the macro-mechanical response. Another material model that may be used to estimate the macro behavior of multi-phase materials is the Gurson model [44, 49, 50]. It has been used to model ductile failure that was characterized by microvoid nucleation and growth [44, 49, 50]. In general, the different material phases are modelled separately with the presumption of perfect interfacial bonding. However, since the microstructure affects the stress states locally [45], interface debonding is one of the primary failure modes noted by other investigators regarding failure of MMCs [46 – 48]. The cohesive zone modelling offers an option to simulate the effect of interfacial debonding [48]. In principle, rather than assuming perfect bonding at the particle-matrix interface, the finite element software-based cohesive zone provides an ability to define a failure criterion to imitate the interfacial debonding. This criterion for the cohesive zone may be either based on the failure stress or failure strain [47, 48]. The application of the cohesive zone modelling to model the interface debonding is promising, but it is restrained due to the challenges in extracting reliable particle-matrix interfacial mechanical properties. Based on the work of Huang, *et al.* [47], it is noted that a high elastic modulus of the cohesive zone results in the fracture of the interface and a low elastic modulus results in the straining of the cohesive zone. Overall, the validated numerical models would expand on understanding of the micro-macro sensitivity between the microstructure and the mechanical properties without the need to perform onerous laboratory experiments.

Finally, this study provides additional insight into the interplay between mechanical behaviour of coatings and spatial variability of properties in the MMC coatings that were fabricated by cold spraying. The high variability may define the challenge in developing and validating the models. As noted, there is high variability in failure strength for approximately the same values of Young's modulus (see Fig. 3). Figure 3a suggests that for the coatings fabricated using a powder blend of 50 wt.% WC + 50 wt.% Ni, they have an average Young's modulus of 121 ± 8 GPa (n = 4). However, the failure strength varied from approximately 38 MPa at 6.35 ± 0.06 wt.% WC in the coating to approximately 77 MPa at 6.89 ± 0.05 wt.% WC in the coating, which represented an approximately 103% variation in strength. Similarly, Fig. 3c suggests that for the coatings fabricated using a powder blend of 92 wt.% WC + 8 wt.% Ni, the average Young's modulus was 231 ± 15 GPa (n = 4). However, the failure strength varied from approximately 168 MPa at 35.67 ± 0.05 wt.% WC in the coating to approximately 276 MPa at 34.92 ± 0.03 wt.% WC in the coating, which represented an approximately 64% variation in failure strength. This high variation in mechanical properties in thermal-sprayed coatings and composites was also noted by Holmberg, *et al.* [29, 30] and Hogan, *et al.* [33, 34]. They explained that the spatial variability included primarily manufacturing defects and pores. These manufacturing defects may degrade the microstructure of the MMC, resulting in composite failure at lower strengths than predicted.

CONCLUSION

In this study, a tensile test was conducted on the cold-sprayed WC-Ni MMC coatings. The mechanical properties of the coating were evaluated by determining Young's modulus, tensile strength, and toughness of the prepared tensile test coupons. The results based on different weight percentages of the WC in the coatings were contrasted, providing a quantitative analysis. This suggested that an increase in the content of WC wt.% in the coatings results in an increase in Young's modulus, tensile strength, and toughness of the coating. This was evident because, with an increase in the content of WC in the coatings, more number of stiffer carbides contributed towards the sharing of external load between the carbide and the metal matrix.

Besides the classical explanation of improvement of mechanical properties due to the increase in the reinforcing particle content, the analysis was also extended to study the effect of the evolved microstructure on the observed tensile strength. The significance of microstructure was comprehended by establishing functional relationship between the tensile strength and the total interfacial area (between particles and metal matrix) per unit thickness, the mean free path, the particle size, and the porosity of the coatings. The results suggest that there is an approximately linear relationship between the tensile strength and the total interfacial area per unit thickness of the coating. The results also indicated that there is a linear relationship between the tensile strength and the inverse of the square root of the mean free path, and the particle size. The tensile strength increases with a decrease in the porosity of the coating, but the data was not scalable. A framework is presented to analyze the combined effect of all the studied microstructural properties on the tensile strength of the coatings. Based on the developed framework, two distinct coating mechanical strength regimes were determined, suggesting a significant increase in the tensile strength of the coatings that were comprised of more than 30 wt.% WC due to the refined microstructure of the coatings. The higher value tensile strength regime was confirmed by the lower damage accumulation and larger average mechanical energy absorbed to failure by the coatings. These quantified and assessed mechanical properties may provide an insight into the load-bearing capacity of the cold-sprayed MMCs. Overall, this study emphasizes the importance of tailoring the microstructure of the cold spray MMC coatings to develop the next generation of coatings with improved mechanical properties and performance.

ACKNOWLEDGEMENT

The authors gratefully acknowledge Mr. David Parlin, a specialist machinist in the Department of Chemical and Materials Engineering at the University of Alberta for machining the parts as required. Special thanks to the Center for Design of Advanced Materials at the University of Alberta for assistance with the high-speed camera assembly and tensile testing. The authors also acknowledge funding support from Imperial Oil (Esso), the Natural Science and Engineering Research Council Canada, the Canada Foundation for Innovation, and the Province of Alberta Ministry of Economic Development, Trade, and Tourism.

REFERENCES

[1] A. Al-Hamed, H. Al-Fadhli, S. Al-Mutairi, B. Yilbas, M. Hashmi, J. Stokes, Investigation of HVOF thermal sprayed nanostructured WC-12Co mixed with Inconel-625 coatings for oil/gas applications, Surf. Eff. Contact Mech. XI WIT Press Southampton (2013) 215–225.

[2] A. Vackel, T. Nakamura, S. Sampath, Mechanical behavior of spray-coated metallic laminates, J. Therm. Spray Technol. 25 (2016) 1009–1019.

[3] G. Smith, O. Higgins, S. Sampath, In-situ observation of strain and cracking in coated laminates by digital image correlation, Surf. Coat. Technol. 328 (2017) 211–218.

[4] G. Smith, S. Sampath, Sustainability of metal structures via spray-clad remanufacturing, J. Miner. Met. Mater. Soc. 70 (2018) 512–520.

[5] I. Hutchings, Tribological properties of metal matrix composites, Mater. Sci. Technol. 10 (1994) 513–517.

[6] N. Chawla, K. Chawla, Microstructure-based modeling of the deformation behavior of particle reinforced metal matrix composites, J. Mater. Sci. 41 (2006) 913–925.

[7] Y. Xie, R. Llewellyn, D. Stiles, Amorphous diamond coating of tungsten carbide and titanium carbonitride for erosive slurry pump component service, Wear 250 (2001) 88–99.

[8] I. Ibrahim, F. Mohamed, E. Lavernia, Particulate reinforced metal matrix composites - A review, J. Mater. Sci. 26 (1991) 1137–1156.

[9] A. Moridi, S. Hassani-Gangaraj, M. Guagliano, M. Dao, Cold spray coating: Review of material systems and future perspectives, Surf. Eng. 30 (2014) 369–395.

[10] P. Fauchais, G. Montavon, Thermal and cold spray: Recent developments, Key Eng. Mater. 384 (2008) 1–59.

[11] N. Chawla, Y. Shen, Mechanical behavior of particle reinforced metal matrix composites, Adv. Eng. Mater. 3 (2001) 357–370.

[12] E. Irissou, J. Legoux, B. Arsenault, C. Moreau, Investigation of Al-Al_2O_3 cold spray coating formation and properties, J. Therm. Spray Technol. 16 (2007) 661–668.

[13] N. Melendez, V. Narulkar, G. Fisher, A. McDonald, Effect of reinforcing particles on the wear rate of low-pressure cold-sprayed WC-based MMC coatings, Wear 306 (2013) 185–195.

[14] Y. Lee, H. Ashrafizadeh, G. Fisher, A. McDonald, Effect of type of reinforcing particles on the deposition efficiency and wear resistance of low-pressure cold-sprayed metal matrix composite coatings, Surf. Coat. Technol. 324 (2017) 190–200.

[15] A. Torrance, Modelling abrasive wear, Wear 258 (2005) 281–293.

[16] N. Melendez, A. McDonald, Development of WC-based metal matrix composite coatings using low-pressure cold gas dynamic spraying, Surf. Coat. Technol. 214 (2013) 101–109.

[17] P. King, S. Zahiri, M. Jahedi, Rare earth/metal composite formation by cold spray, J. Therm. Spray Technol. 17 (2008) 221–227.

[18] T. Gustafson, P. Panda, G. Song, R. Raj, Influence of microstructural scale on plastic flow behavior of metal matrix composites, Acta Mater. 45 (1997) 1633–1643.

[19] I. Lee, C. Hsu, C. Chen, N. Ho, P. Kao, Particle-reinforced aluminum matrix composites produced from powder mixtures via friction stir processing, Compos. Sci. Technol. 71 (2011) 693–698.

[20] M. Kouzeli, A. Mortensen, Size dependent strengthening in particle reinforced aluminum, Acta Mater. 50 (2002) 39–51.

[21] A. Basak, A. Pramanik, C. Prakash, Deformation and strengthening of SiC reinforced Al-MMCs during in-situ micro-pillar compression, Mater. Sci. Eng. A 763 (2019) 138141.

[22] Y. Su, Q. Ouyang, W. Zhang, Z. Li, Q. Guo, G. Fan, D. Zhang, Composite structure modeling and mechanical behavior of particle reinforced metal matrix composites, Mater. Sci. Eng. A 597 (2014) 359–369.

[23] K. Hodder, H. Izadi, A. McDonald, A. Gerlich, Fabrication of aluminum–alumina metal matrix composites via cold gas dynamic spraying at low pressure followed by friction stir processing, Mater. Sci. Eng. A 556 (2012) 114–121.

[24] A. Griffith, The phenomena of rupture and flow in solids, Philos. Trans. Royal Soc. London A 221 (1921) 163–198.

[25] W. Smith, J. Hashemi, Foundations of Materials Science and Engineering, sixth ed., McGraw-Hill, New York, 2006.

[26] X-T. Luo, G-J. Yang, C-J. Li, Multiple strengthening mechanisms of cold-sprayed cBNp/NiCrAl composite coating, Surf. Coat. Technol. 205 (2011) 4808–4813.

[27] X-T. Luo, C-J. Li, Large sized cubic BN reinforced nanocomposite with improved abrasive wear resistance deposited by cold spray, Mater. Des. 83 (2015) 249–256.

[28] C. Nan, D. Clarke, The influence of particle size and particle fracture on the elastic/plastic deformation of metal matrix composites, Acta Mater. 44 (1996) 3801–3811.

[29] K. Holmberg, A. Laukkanen, E. Turunen, T. Laitinen, Wear resistance optimisation of composite coatings by computational microstructural modelling, Surf. Coat. Technol. 247 (2014) 1–13.

[30] K. Holmberg, A. Laukkanen, A. Ghabchi, M. Rombouts, E. Turunen, R. Waudby, T. Suhonen, K. Valtonen, E. Sarlin, Computational modelling based wear resistance analysis of thick composite coatings, Tribol. Int. 72 (2014) 13–30.

[31] S. Leigh, C. Lin, C. Berndt, Elastic response of thermal spray deposits under indentation tests, J. Am. Ceram. Soc. 80 (1997) 2093–2099.

[32] W. Choi, L. Li, V. Luzin, R. Neiser, T. Gnaupel-Herold, H. J. Prask, S. Sampath, A. Gouldstone, Integrated characterization of cold sprayed aluminum coatings, Acta Mater. 55 (2007) 857–866.

[33] J. Hogan, L. Farbaniec, T. Sano, M. Shaeffer, K. Ramesh, The effects of defects on the uniaxial compressive strength and failure of an advanced ceramic, Acta Mater. 102 (2016) 263–272.

[34] J. Hogan, L. Farbaniec, N. Daphalapurkar, K. Ramesh, On compressive brittle fragmentation, J. Am. Ceram. Soc. 99 (2016) 2159–2169.

[35] ASTM E8/E8M-13a, Standard Test Methods for Tension Testing of Metallic Materials, ASTM International, West Conshohocken, USA, 2013.

[36] A. Abedini, Z. Chen, A micromechanical model of particle-reinforced metal matrix composites considering particle size and damage, Comput. Mater. Sci. 85 (2014) 200–205.

[37] G. Nelson, J. Nychka, A. McDonald, Structure, phases, and mechanical response of Ti-alloy bioactive glass composite coatings, Mater. Sci. Eng. C 36 (2014) 261–276.

[38] D. McDanels, Analysis of stress-strain, fracture and ductility behaviour of aluminium matrix composites containing discontinuous SiC reinforcement, Metall. Trans. A 16A (1985) 1105–1115.

[39] M. P. Dewar, A. G. McDonald, A. P. Gerlich, Interfacial heating during low-pressure cold-gas dynamic spraying of aluminum coatings, J. Mater. Sci. 47 2012 184–198.

[40] P. Singh, J. Lewandowski, Scr. Mater. 29 (1993) 199–204.

[41] G. Greaves, A. Greer, R. Lakes, T. Rouxel, Poisson’s ratio and modern materials, Nat. Mater. 10 (2011) 823–837.

[42] H. Gercek, Poisson's ratio values for rocks, Int. J. Rock Mech. Mining Sci. 44 (2007) 1–13.

[43] G. Bae, Y. Xiong, S. Kumar, K. Kang, C. Lee, General aspects of interface bonding in kinetic sprayed coatings, Acta Mater. 56 (2008) 4858–4868.

[44] Z. Zhang, C. Thaulow, J. Edegard, Eng. Fracture Mech. 67 (2000) 155–168.

[45] A. Shedbale, I. Singh, B. Mishra, Heterogeneous and homogenized models for predicting the indentation response of particle reinforced metal matrix composites, Int. J. Mech. Mater. Des. 13 (2017) 531–552.

[46] P. Kanouté, D. Boso, J. Chaboche, B. Schrefler, Multiscale methods for composites: A review, Arch. Comput. Methods Eng. 16 (2009) 31–75.

[47] J. Huang, G. Wu, W. Sha, Finite element modeling of properties influence of particle characteristics in particle reinforced metal matrix composite, Compos. Nanocompos. (2013) 1–20.

[48] T. Sadowski, B. Pankowski, Numerical modelling of two-phase ceramic composite response under uniaxial loading, Compos. Struct. 143 (2016) 388–394.

[49] A. Gurson, Continuum theory of ductile rupture by void nucleation and growth: Part I: Yield criteria and flow rules for porous ductile media, J. Eng. Mater. Technol. 99 (1977) 2–15.

[50] B. Amirian, H. Li, J. Hogan, An experimental and numerical study of novel nanograined (γ + α_2)-TiAl/Al_2O_3 cermets, Mater. Sci. Eng. A. 744 (2019) 570–580.

LIST OF FIGURE AND TABLE CAPTIONS

Figure 1: SEM images of the microstructure of cold-sprayed MMC coatings fabricated from (*a*) 50 wt.% WC + 50 wt.% Ni powder blend, (*b*) 71 wt.% WC + 29 wt.% Ni powder blend, and (*c*) 92 wt.% WC + 8 wt.% Ni powder blend.

Figure 2: Plot of WC weight fraction in the MMC coating as a function of WC weight fraction in the cold-sprayed feed powder blend.

Figure 3: Tensile stress versus tensile strain of cold-sprayed MMC coatings fabricated from (*a*) 50 wt.% WC + 50 wt.% Ni powder blend, (*b*) 71 wt.% WC + 29 wt.% Ni powder blend, (*c*) and 92 wt.% WC + 8 wt.% Ni powder blend. The final wt.% of WC in the coating is as indicated in the legend insert.

Figure 4: Tensile strength of cold-sprayed MMC coatings as a function of the total interfacial area per unit thickness (Ψ) between the WC reinforcing particles and the metal matrix. The wt.% of the WC in the coating is indicated on the curve.

Figure 5: Tensile strength of cold-sprayed MMC coatings as a function of the inverse square root of the mean free path (λ). The wt.% of the WC in the coating is indicated on the curve.

Figure 6: High magnification SEM micrographs showing the irregular morphology of the deposited WC particles at (*a*) 500X and (*b*) 2000X.

Figure 7: Tensile strength of cold-sprayed MMC coatings as a function of the average particle size (ϕ). The wt.% of the WC in the coating is indicated on the curve.

Figure 8: Tensile strength of cold-sprayed MMC coatings as a function of the inverse of porosity (θ). The wt.% of the WC in the coating is indicated on the curve.

Figure 9: Tensile strength of cold-sprayed WC-Ni MMC coatings as a function of the independent variables of interfacial area, mean free path, average particle size, and coating porosity.

Figure 10: Lateral strain of cold-sprayed MMC coatings as a function of the axial strain. (*a*) Plot presenting the curves for the full duration of tensile testing, and (*b*) Plot presenting the curves for the initial stage of tensile testing. The solid curves represent the content of WC in the coating was less than 15 wt.% and the dashed curves represent the content of WC was more than 30 wt.% in the coating. The percentage porosity in the coating is indicated on the curve.

TABLES

Table 1: Cold spray deposition parameters for 50 wt.% WC + 50 wt.% Ni powder blend, 71 wt.% WC + 29 wt.% Ni powder blend, and 92 wt.% + 8wt.% Ni powder blend.

Process Parameter	**Value**
Process Gas	Compressed air
Compressed Air Pressure	634 kPa
Compressed Air Temperature	550°C
Stand-off Distance	5 mm
Nozzle velocity	5 mm/s

Table 2: Content of WC wt.%, tensile strength, Young's modulus, failure strain, and toughness of the fabricated MMC coatings.

wt.% WC in coating (n = 25)	Tensile strength (MPa)	Young's modulus (GPa)	Failure strain (%)	Toughness (N/mm^2)
6.35 ± 0.06	38	121	0.036	0.006
6.45 ± 0.11	72	114	0.082	0.033
6.89 ± 0.05	77	133	0.084	0.023
7.69 ± 0.07	68	116	0.079	0.03
10.99 ± 0.07	111	123	0.101	0.062
11.47 ± 0.04	110	137	0.113	0.071
13.69 ± 0.03	128	152	0.089	0.061
14.78 ± 0.04	131	150	0.086	0.06
34.92 ± 0.03	276	233	0.140	0.199
35.67 ± 0.05	168	210	0.092	0.063
37.78 ± 0.04	257	247	0.123	0.167
40.47 ± 0.03	220	235	0.101	0.109

Table 3: Content of WC wt.%, total interfacial area per unit thickness, mean free path, average reinforcing particle size, and porosity of the fabricated MMC coatings.

wt.% WC in coating (n = 25)	Total interfacial area per unit thickness (µm) (n = 25)	Mean free path (µm) (n = 25)	Average reinforcing particle size (µm^2) (n = 25)	Porosity (%) (n = 25)
6.35 ± 0.06	5586 ± 147	83 ± 10	19.37 ± 0.44	0.48 ± 0.03
6.45 ± 0.11	8253 ± 133	75 ± 10	19.27 ± 0.48	0.35 ± 0.03
6.89 ± 0.05	8273 ± 209	79 ± 9	18.02 ± 0.30	0.41 ± 0.02
7.69 ± 0.07	7018 ± 214	54 ± 6	18.33 ± 0.7	0.34 ± 0.03
10.99 ± 0.07	9901 ± 128	42 ± 5	13.27 ± 0.34	0.45 ± 0.11
11.47 ± 0.04	9867 ± 115	44 ± 6	14.54 ± 0.35	0.42 ± 0.06
13.69 ± 0.03	10032 ± 129	38 ± 4	11.84 ± 0.27	0.30 ± 0.03
14.78 ± 0.04	11922 ± 196	36 ± 4	12.17 ± 0.31	0.32 ± 0.02
34.92 ± 0.03	42834 ± 3960	13 ± 0.4	7.24 ± 0.31	0.037 ± 0.004
35.67 ± 0.05	30001 ± 2774	15 ± 0.8	9.03 ± 0.16	0.048 ± 0.001
37.78 ± 0.04	37106 ± 9811	12 ± 0.4	8.64 ± 0.29	0.042 ± 0.005
40.47 ± 0.03	35524 ± 3960	13 ± 0.2	9.19 ± 0.33	0.049 ± 0.006

Figure 1a

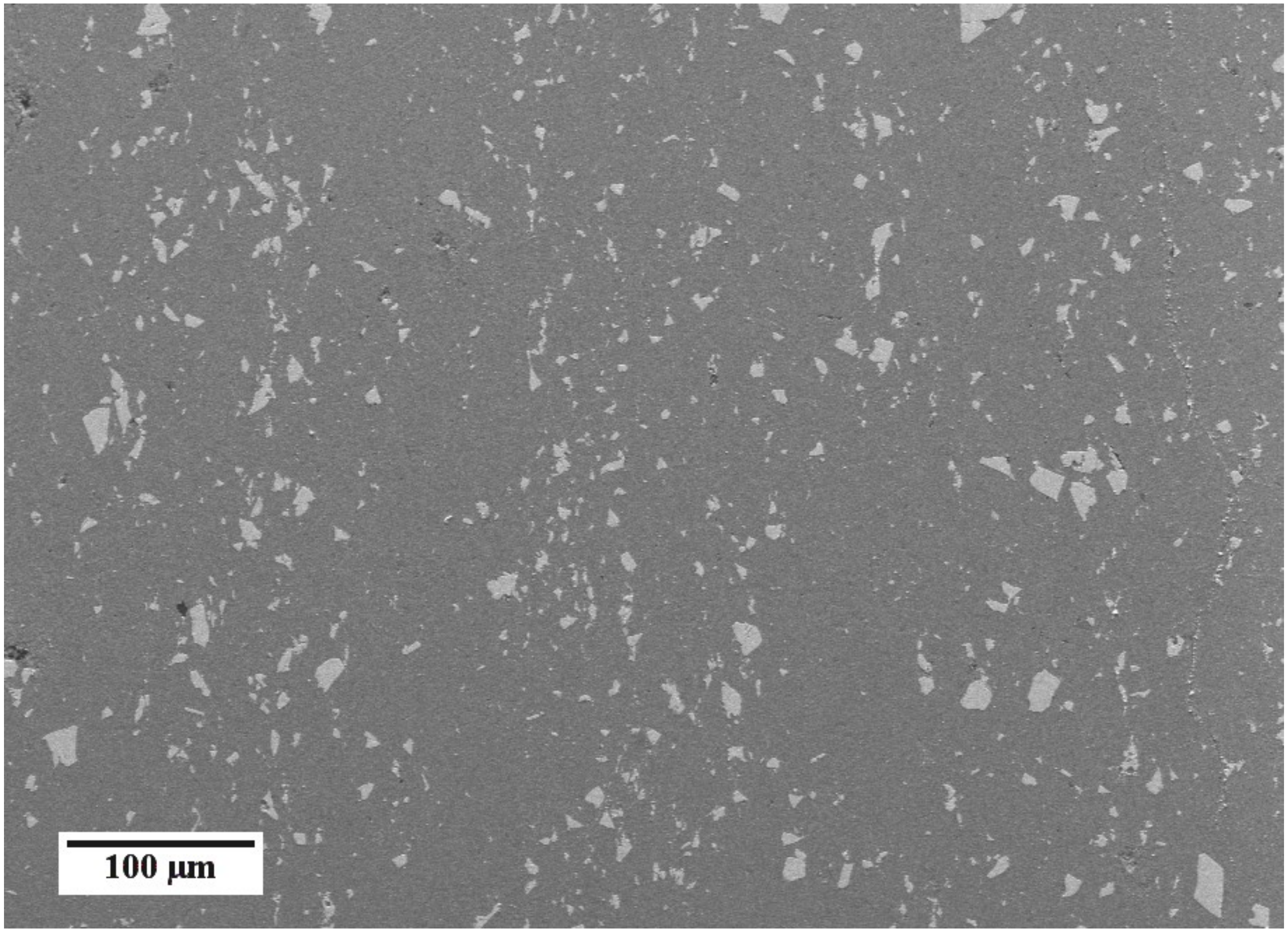

Figure 1b

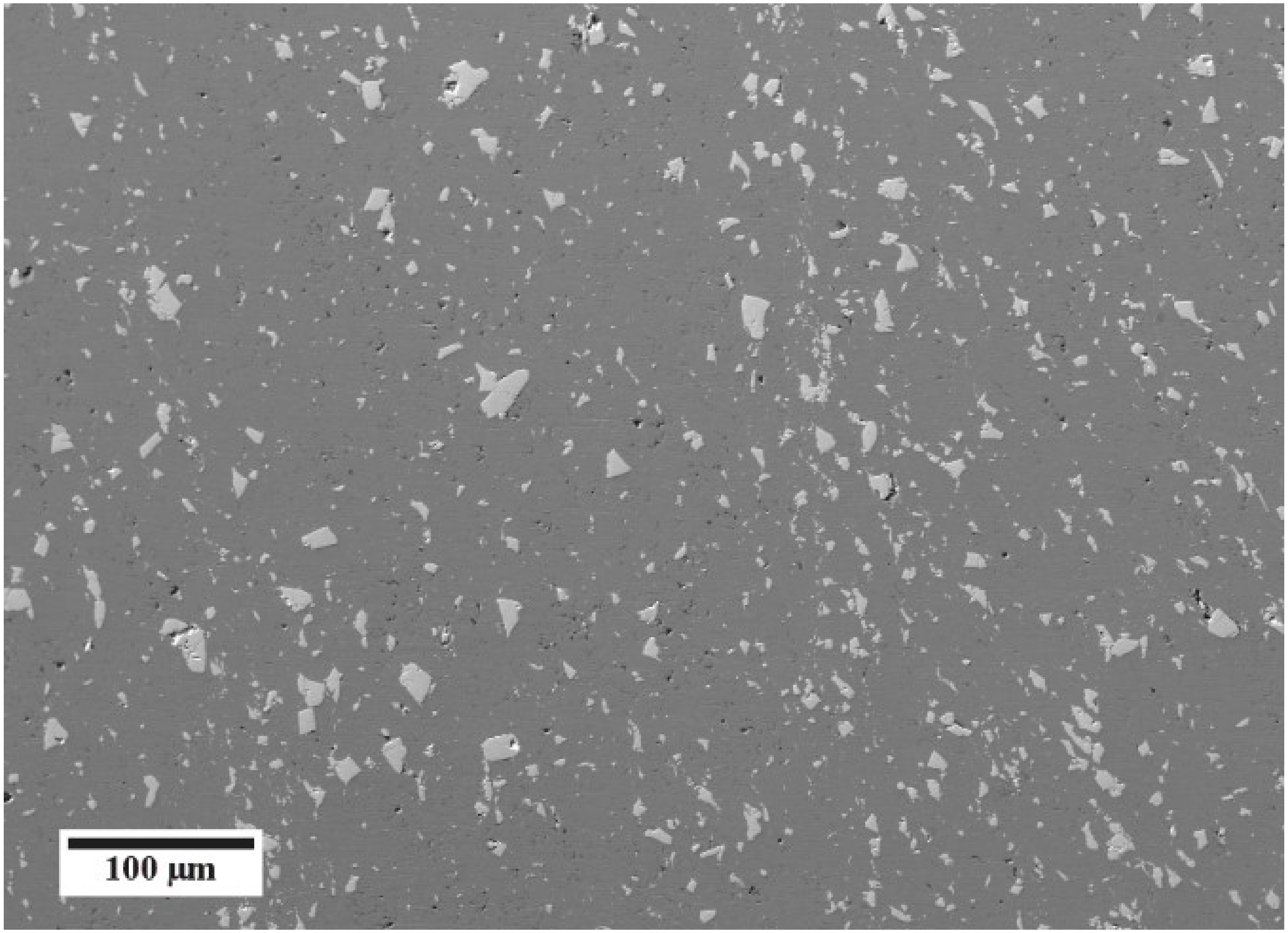

Figure 1c

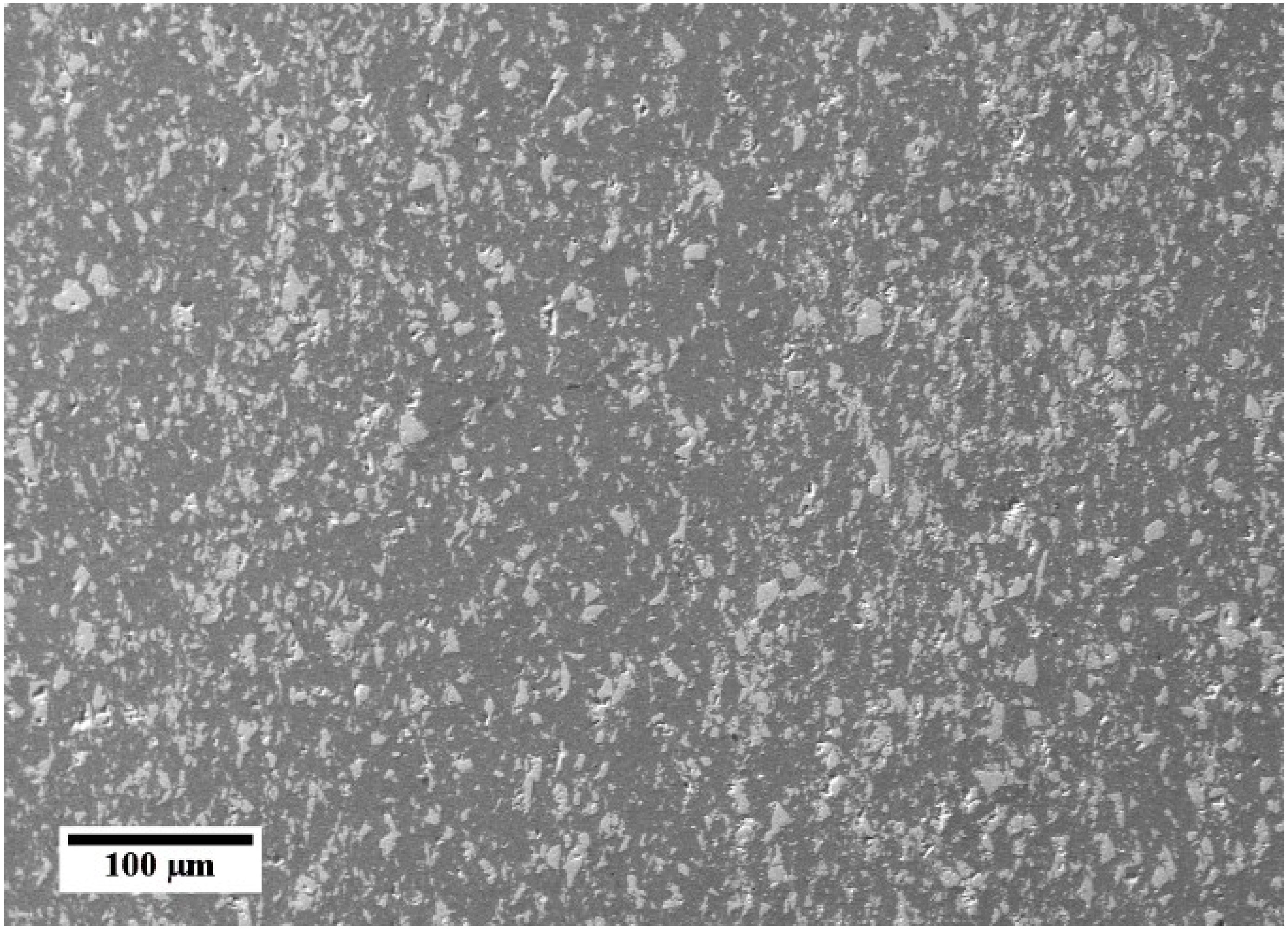

Figure 2

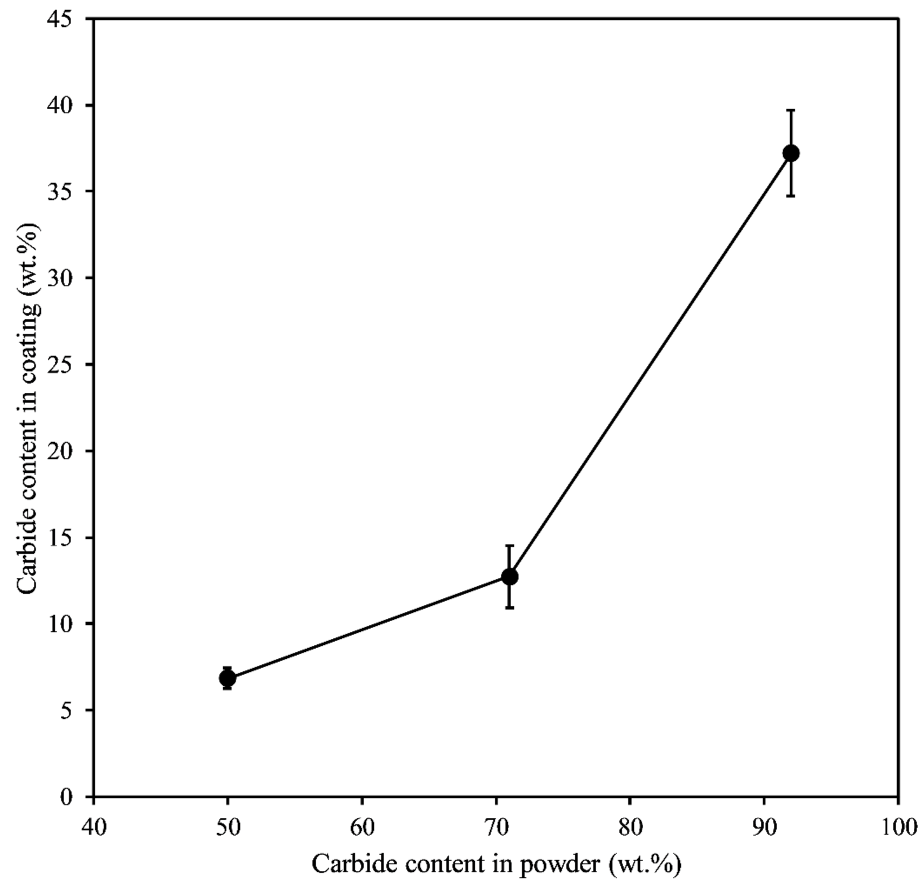

45
40
35
30
25
20
15
10
5
0
Carbide content in coating (wt.%)
40
50
60
70
80
90
100
Carbide content in powder (wt.%)

Figure 3a

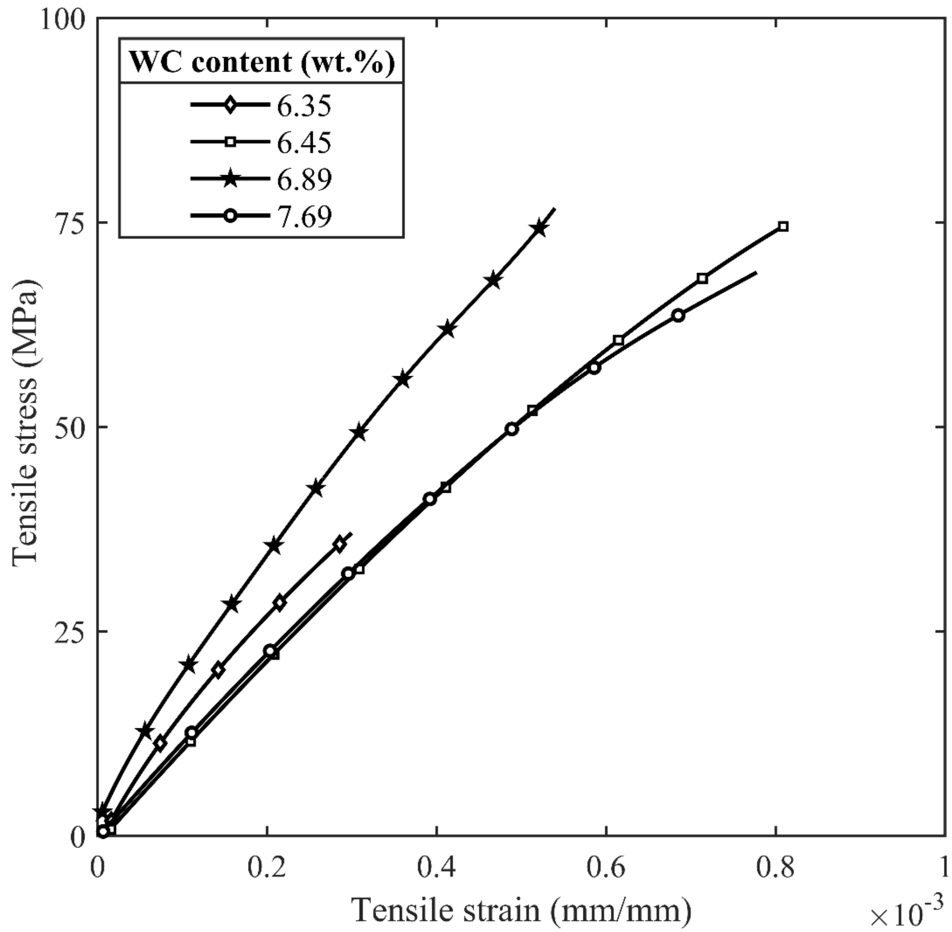

WC content (wt.%)
6.35
6.45
6.89
7.69
Tensile stress (MPa)
100
75
50
25
0
0
0.2
0.4
0.6
0.8
1
Tensile strain (mm/mm)
$\times 10^{-3}$

Figure 3b

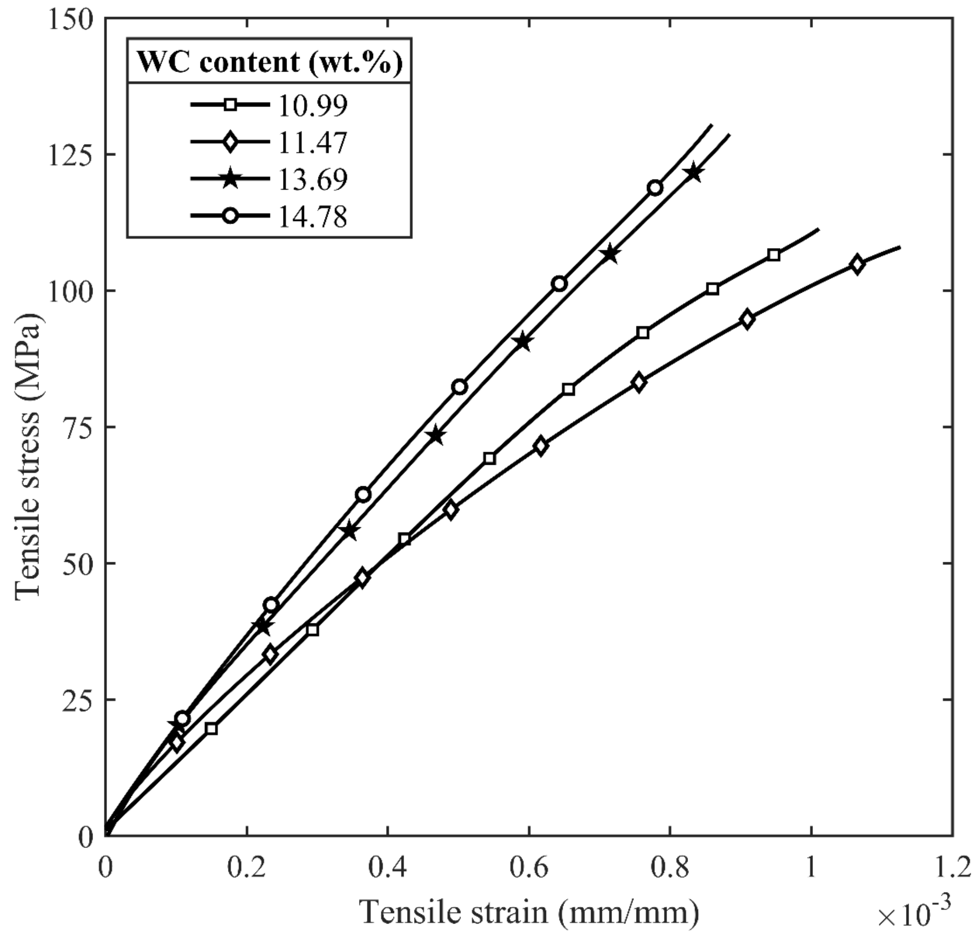

WC content (wt.%)
10.99
11.47
13.69
14.78
Tensile stress (MPa)
Tensile strain (mm/mm)
$\times 10^{-3}$
150
125
100
75
50
25
0
0
0.2
0.4
0.6
0.8
1
1.2

Figure 3c

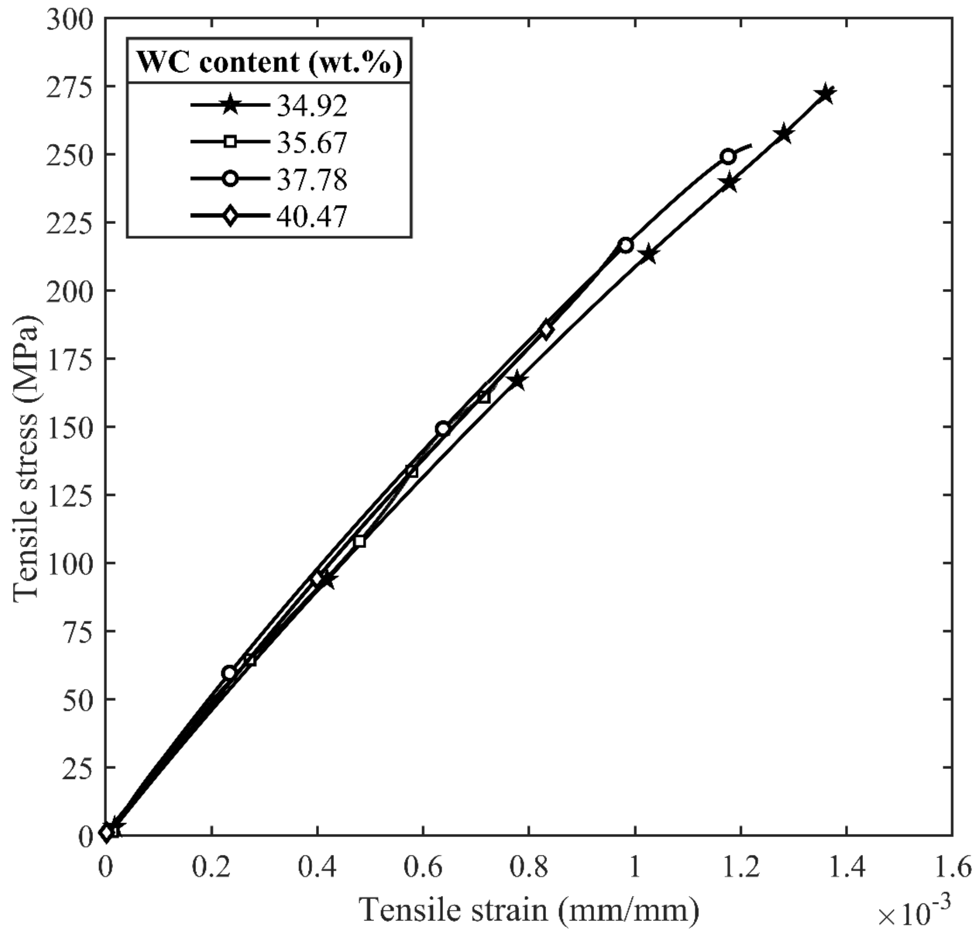
WC content (wt.%)
34.92
35.67
37.78
40.47
Tensile stress (MPa)
Tensile strain (mm/mm)
$\times 10^{-3}$
0
25
50
75
100
125
150
175
200
225
250
275
300
0
0.2
0.4
0.6
0.8
1
1.2
1.4
1.6

Figure 4

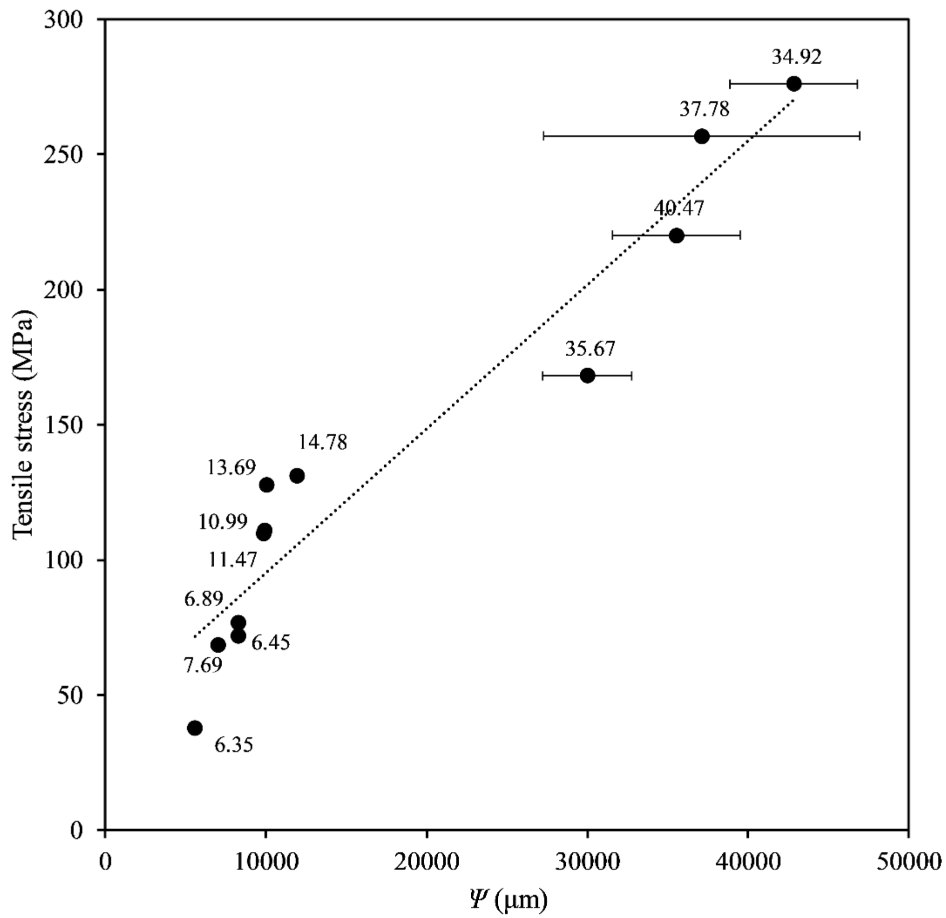

300
250
200
150
100
50
0
Tensile stress (MPa)
0
10000
20000
30000
40000
50000
Ψ (µm)
34.92
37.78
40.47
35.67
14.78
13.69
10.99
11.47
6.89
6.45
7.69
6.35

Figure 5

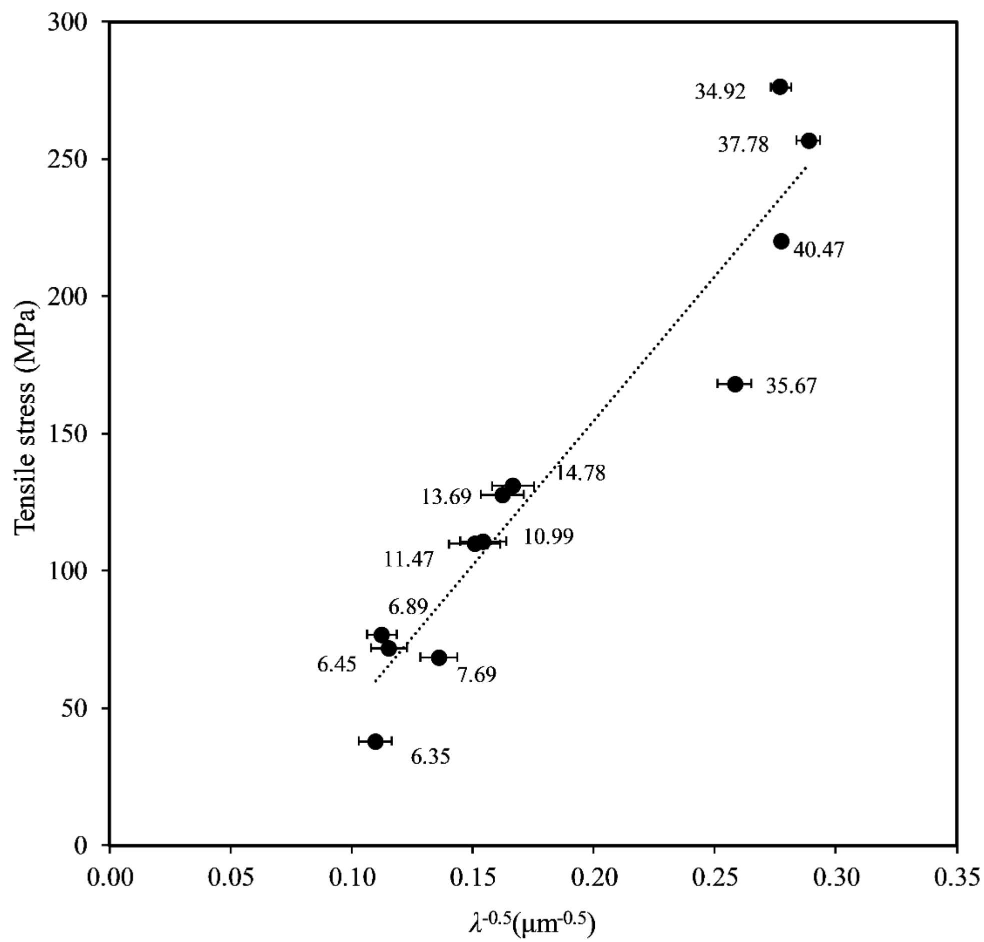

300
250
200
150
100
50
0
0.00
0.05
0.10
0.15
0.20
0.25
0.30
0.35
Tensile stress (MPa)
λ-0.5(μm-0.5)
34.92
37.78
40.47
35.67
14.78
13.69
10.99
11.47
6.89
6.45
7.69
6.35

Figure 6a

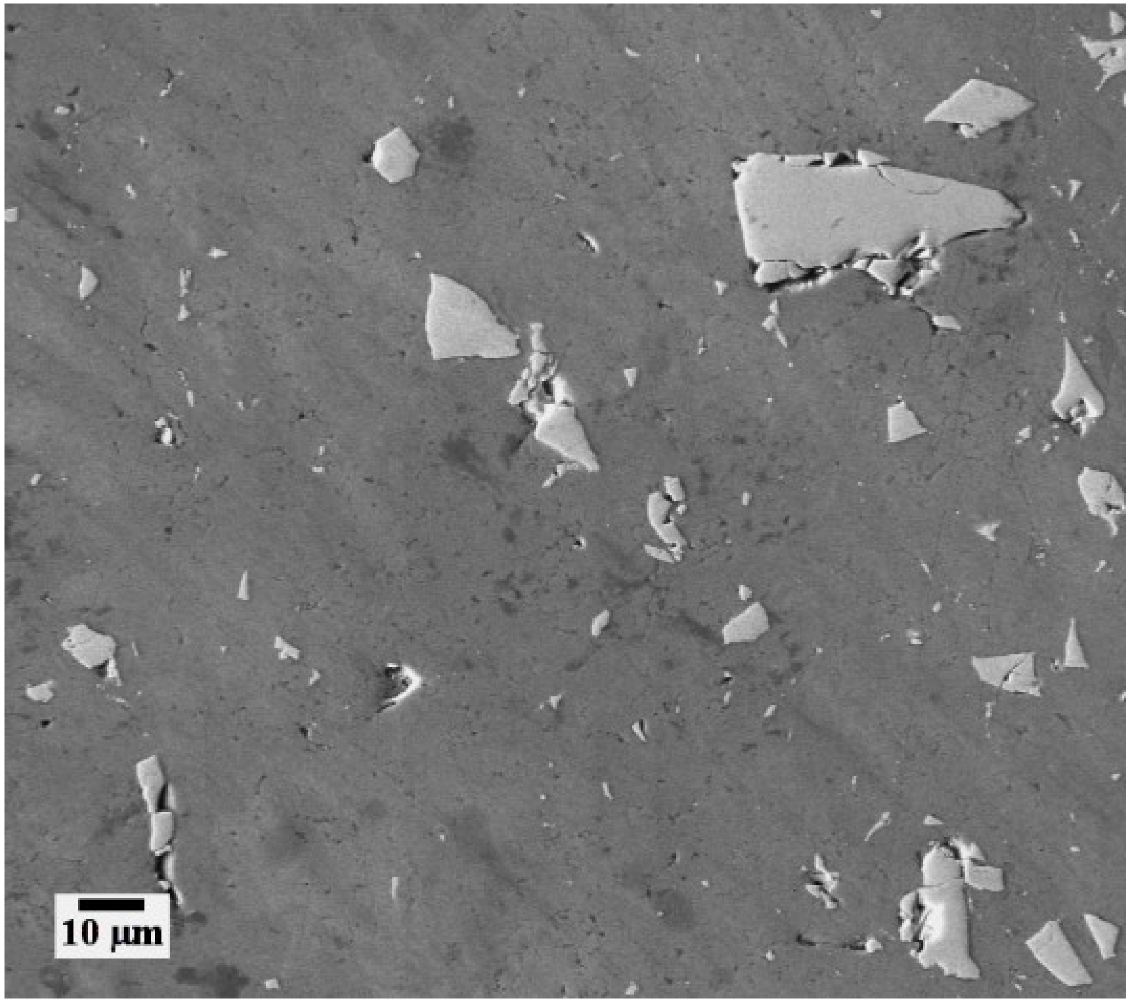

Figure 6b

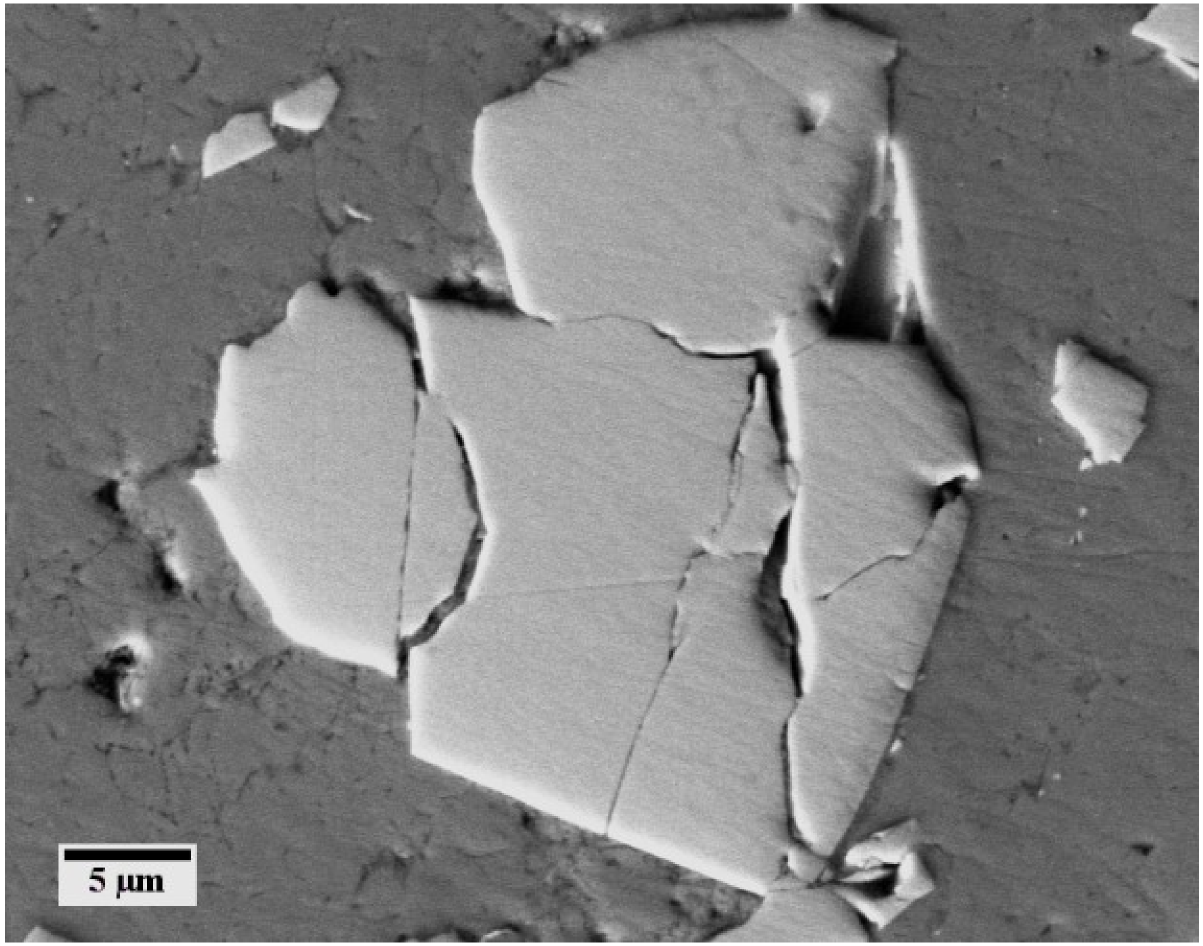

Figure 7

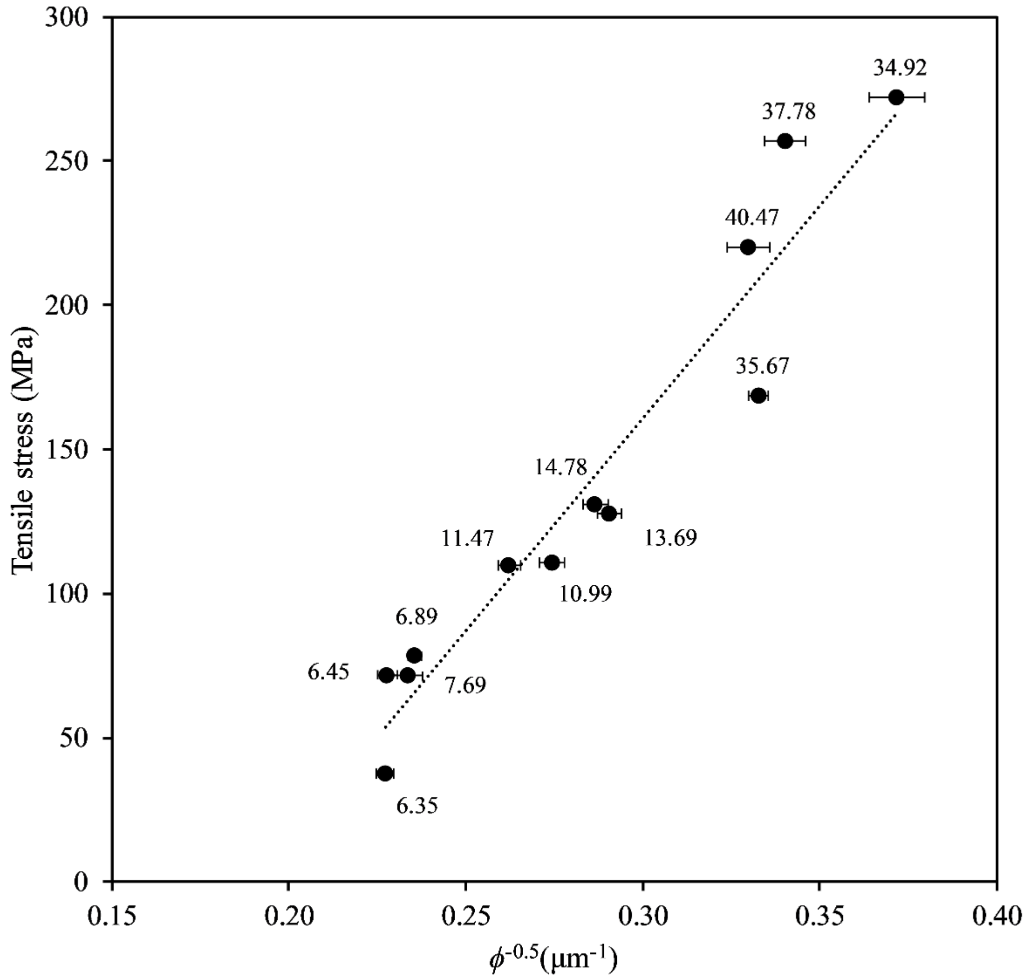
300
250
200
150
100
50
0
0.15
0.20
0.25
0.30
0.35
0.40
Tensile stress (MPa)
ϕ-0.5(μm-1)
34.92
37.78
40.47
35.67
14.78
13.69
11.47
10.99
6.89
6.45
7.69
6.35

Figure 8

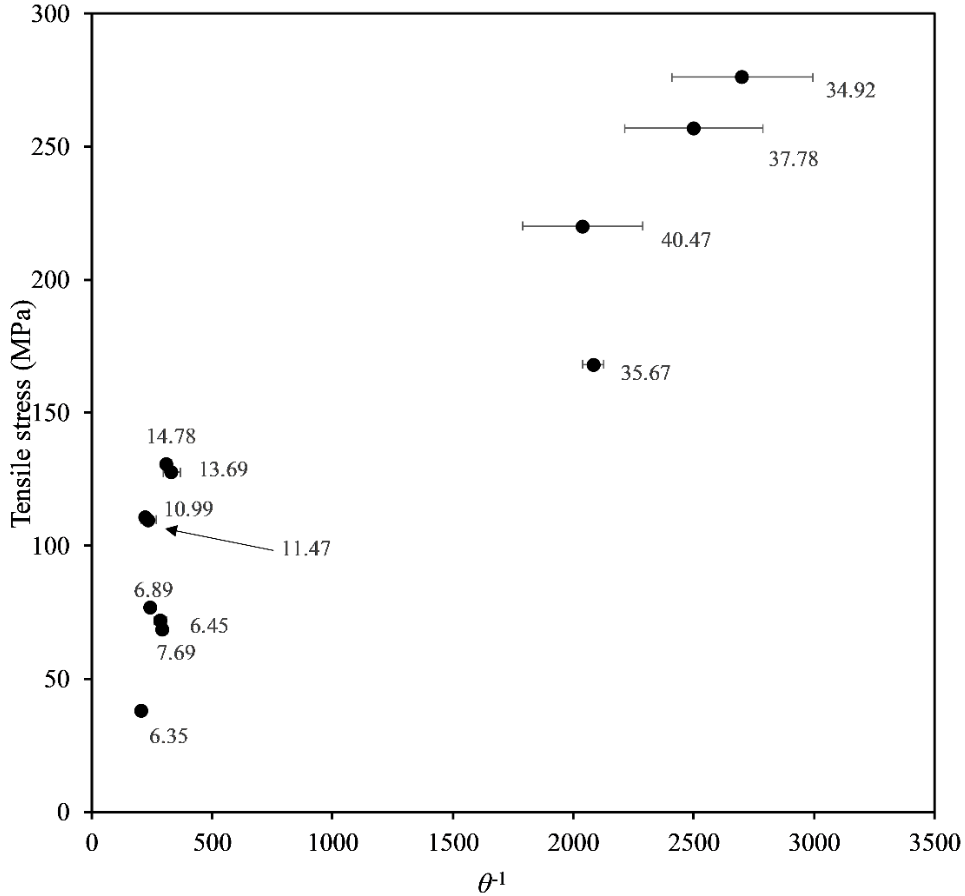

Tensile stress (MPa)
300
250
200
150
100
50
0
0
500
1000
1500
2000
2500
3000
3500
θ^{-1}
34.92
37.78
40.47
35.67
14.78
13.69
10.99
11.47
6.89
6.45
7.69
6.35

Figure 9

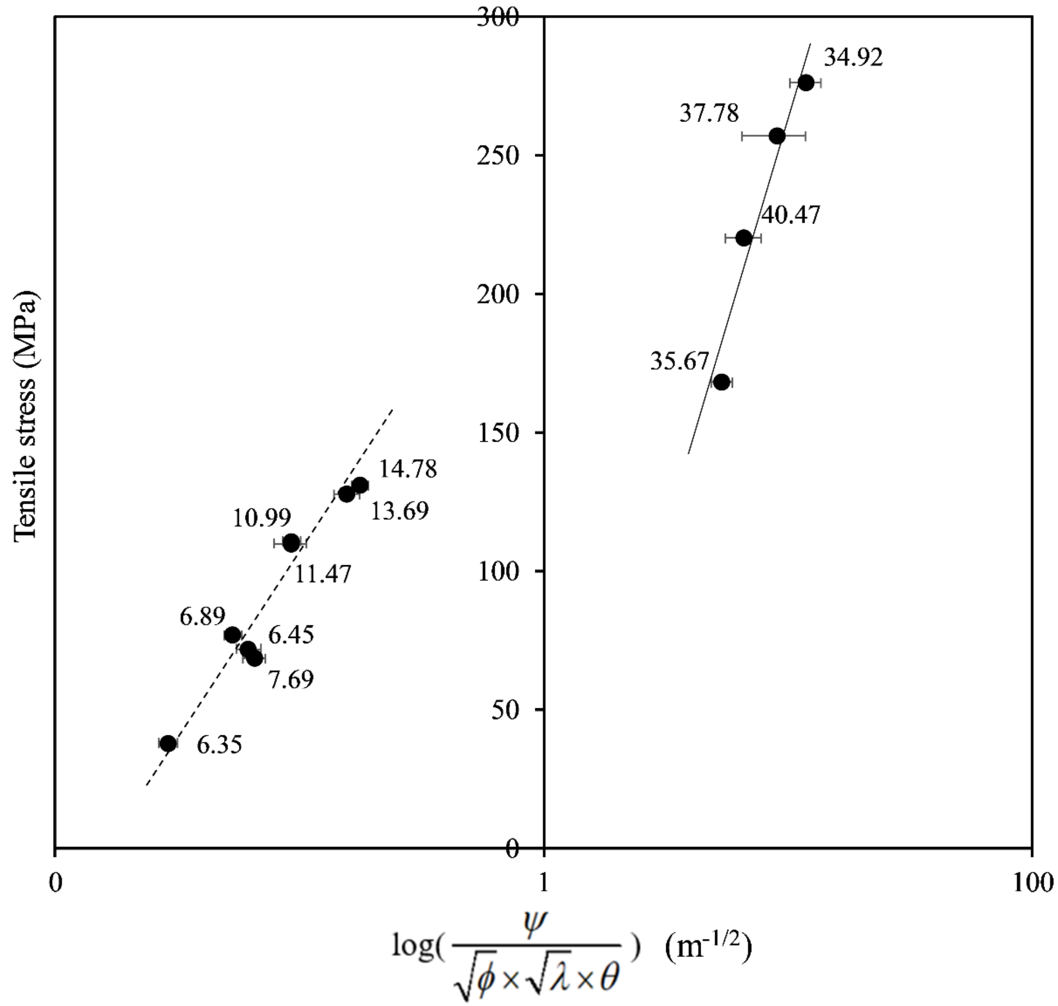

Tensile stress (MPa)
300
250
200
150
100
50
0
0
1
100
34.92
37.78
40.47
35.67
14.78
13.69
10.99
11.47
6.89
6.45
7.69
6.35
$\log(\frac{\psi}{\sqrt{\phi}\times\sqrt{\lambda}\times\theta})$ ($m^{-1/2}$)

Figure 10a

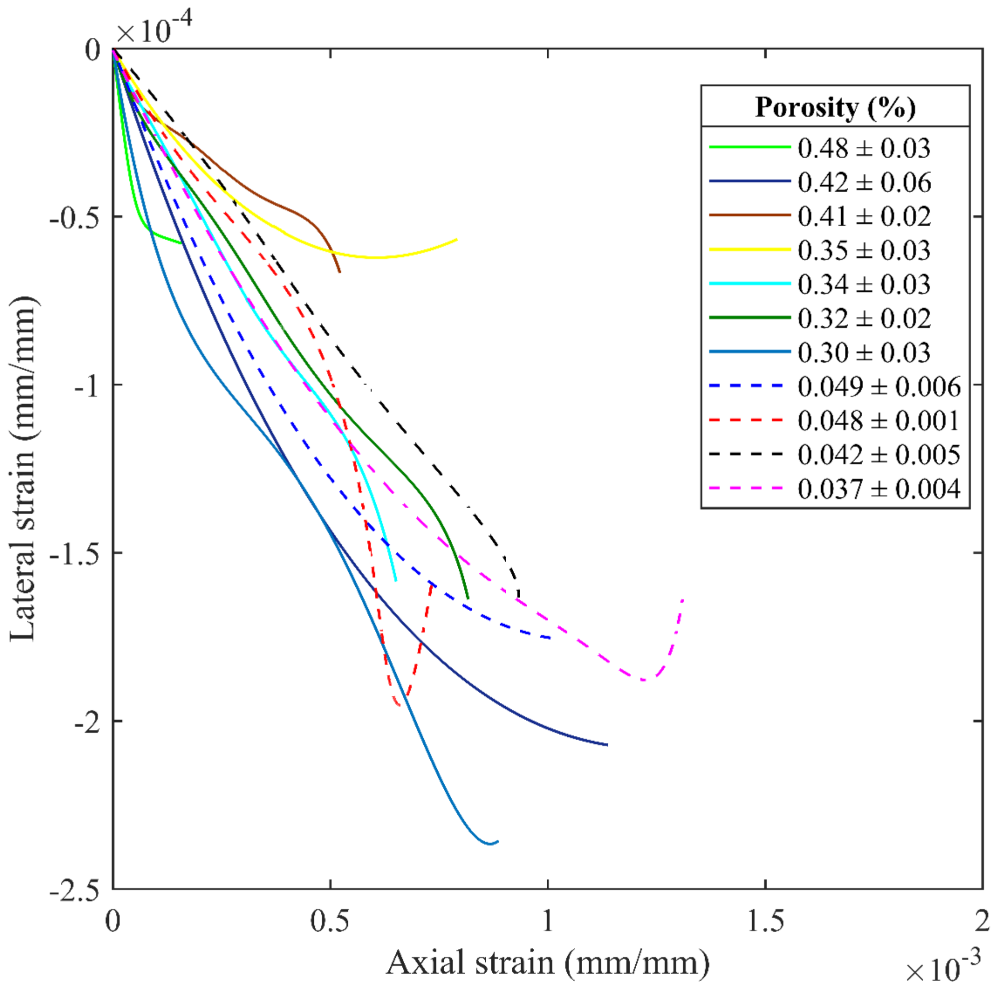

×10-4
0
-0.5
-1
-1.5
-2
-2.5
Lateral strain (mm/mm)
0
0.5
1
1.5
2
Axial strain (mm/mm)
×10-3
Porosity (%)
0.48 ± 0.03
0.42 ± 0.06
0.41 ± 0.02
0.35 ± 0.03
0.34 ± 0.03
0.32 ± 0.02
0.30 ± 0.03
0.049 ± 0.006
0.048 ± 0.001
0.042 ± 0.005
0.037 ± 0.004

Figure 10b

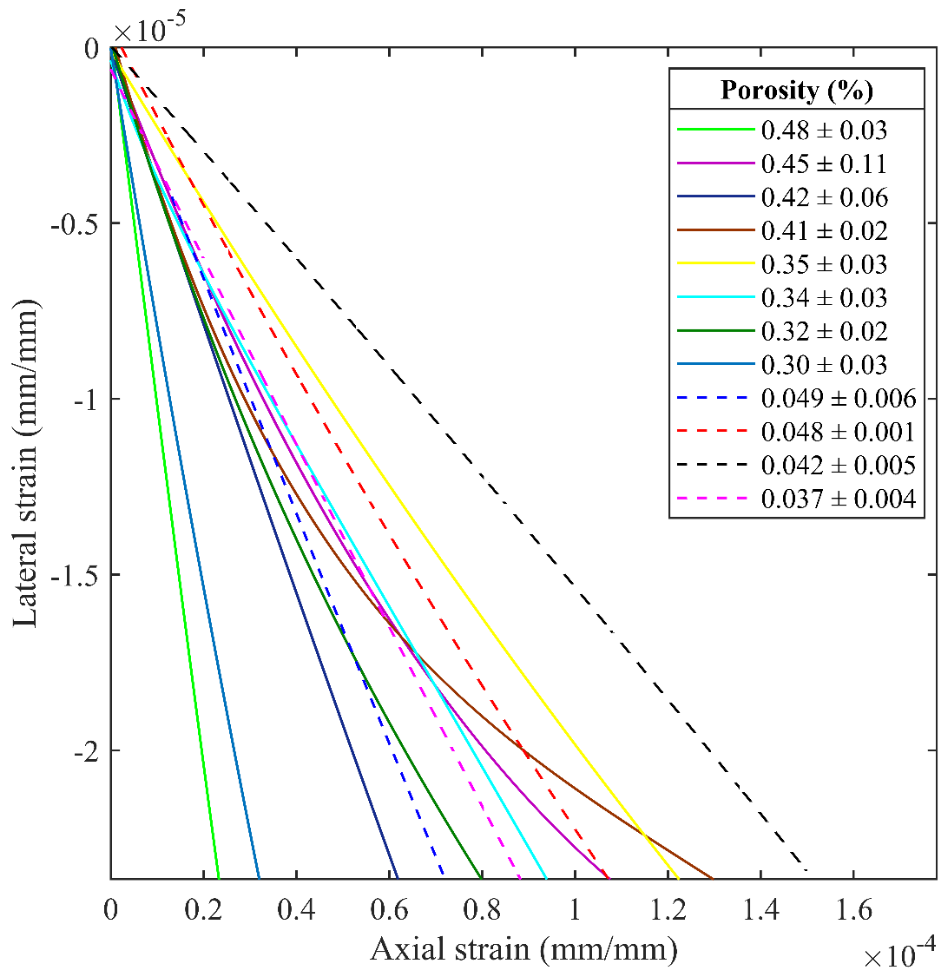

Porosity (%)
0.48 ± 0.03
0.45 ± 0.11
0.42 ± 0.06
0.41 ± 0.02
0.35 ± 0.03
0.34 ± 0.03
0.32 ± 0.02
0.30 ± 0.03
0.049 ± 0.006
0.048 ± 0.001
0.042 ± 0.005
0.037 ± 0.004
Lateral strain (mm/mm)
Axial strain (mm/mm)
×10^-5
×10^-4
0
-0.5
-1
-1.5
-2
0
0.2
0.4
0.6
0.8
1
1.2
1.4
1.6